

THERMAL ANALOGY FOR THE DIFFUSION OF NEUTRONS
IN A TWO CORE REACTOR

by

Dwyla Justine Tunstall

A Thesis Submitted to the
Graduate Faculty in Partial Fulfillment of
The Requirements for the Degree of
MASTER OF SCIENCE

Major Subject: Nuclear Engineering

Signatures have been redacted for privacy

Iowa State University
Of Science and Technology
Ames, Iowa
1970

TABLE OF CONTENTS

INTRODUCTION	1
THEORETICAL DEVELOPMENT OF THE THERMAL ANALOGY	4
Derivation of Prototype and Model Characteristic Equations	4
Establishment of the Relationship Between the Characteristic Equations	12
Boundary Conditions Considerations	14
ACTUAL MODEL DESIGN	19
Materials Selection	19
Determination of Desirable Design Parameters	20
Model Construction	27
METHOD OF TAKING DATA AND PLOTS OF RESULTS	33
DISCUSSION OF RESULTS AND ERROR CONSIDERATIONS	65
CONCLUSIONS	73
RECOMMENDATIONS FOR FURTHER STUDY	74
LITERATURE CITED	75
ACKNOWLEDGEMENTS	76
APPENDIX	77
List of Symbols and Definitions	77
Experimental Data and Peak Ratio Calculations	80
List of Equipment	88

INTRODUCTION

For safety and control purposes it is important to know the response of a reactor to small perturbations in reactivity, and to know the response of a detector to the variations in the neutron flux at various locations in the reactor. Many studies (1) have concerned the response of the reactor to sinusoidal variations from the steady state system. Experimentally the macroscopic absorption cross section is caused to vary sinusoidally with the use of an oscillator or neutron pulses are introduced. These can be reduced analytically to a series of sinusoidal changes in reactivity. When a sinusoidal variation in reactivity is introduced in the reactor, the measured reactor response is also sinusoidal, but of different magnitude and phase. From

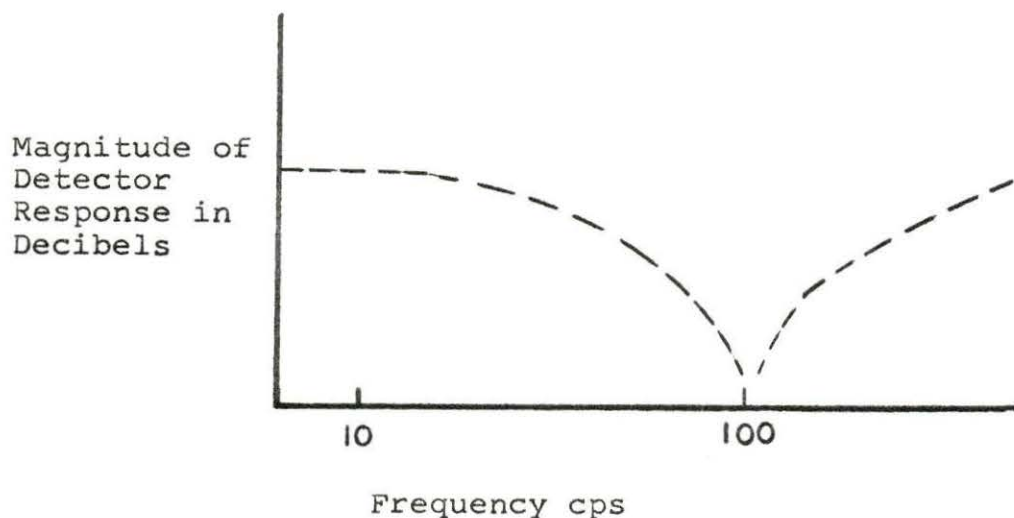


Figure 1. Magnitude of detector response versus frequency for a location in the UTR-10

frequency studies (5) in the two-core UTR-10 reactor, a so called 'dead spot' or position in the reactor was found at which the response of a detector to the neutron flux dies out. This was observed at certain frequencies called sink frequencies, the first occurring at approximately one hundred cycles per second. In these experiments the oscillator was placed in an outer graphite region adjacent to the two cores and detectors were placed at other locations. Figure 1 (5) shows the nature of the detector response in the vicinity of the first sink frequency. From a safety point of view a lack of response from a detector at certain frequencies and locations in the reactor could result in a serious situation.

The object of this thesis is to investigate the applicability of a thermal model of the neutron flux to study the sink phenomenon. An analogy is established between a two-core reactor prototype and a thermal model; the theory of similitude establishes the conditions under which they are similar, and provides the approach to studying one in terms of the other. From the thermal model, with the analogy that conduction of heat pulses down a metal rod is similar to neutron pulses in the UTR-10, a study was made to reproduce the sink frequency behavior in the model and hence learn more about its nature in the real reactor system.

In developing the thermal analogy it is necessary to

consider the characteristic equations that describe the reactor system and those proposed for the analog, and to determine the conditions under which they satisfy similitude requirements. The analog consists of a rod with two heat-source sections, separated by sections without heat sources, to represent fuel and graphite regions of the two-core reactor. A temperature pulse driver on one end of the rod is analogous to the oscillator in the reactor system superimposing a rectified sine temperature variation on the steady state condition. As in the reactor, the frequency response of the model is also sinusoidal, but of different magnitude and phase. Thermistors are placed along the rod to correspond to the neutron detectors in the reactor prototype.

THEORETICAL DEVELOPMENT OF THE THERMAL ANALOGY

Derivation of Prototype and Model
Characteristic Equations

In this development of the characteristic equations governing the reactor, one-group theory is assumed to be valid. Neutrons are assumed to travel at the most probable thermal velocity (v) as predicted from the Maxwell-Boltzmann distribution for room temperature. Further simplification includes considering only the one-dimensional differential diffusion equation for the flux distribution in the unsteady state. In considering a two-core, heterogeneous reactor such as the UTR-10, two basic regions are recognized - the fuel regions and the graphite reflector sections. The reactor is moderated by light water in the two core tank regions.

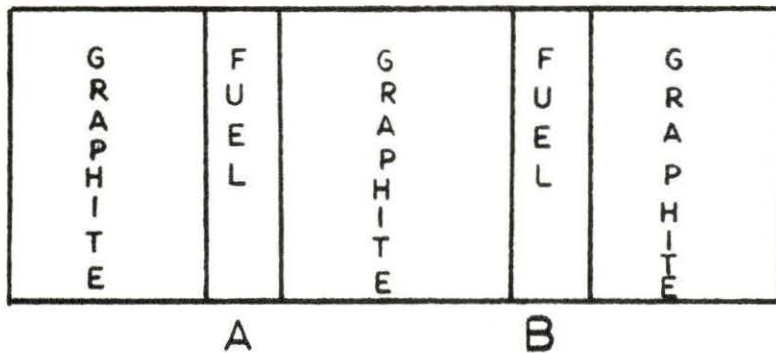


Figure 2. Sketch of UTR-10

Neither core A nor core B can achieve criticality alone, but only with additional contributions of neutrons from one another. From the application of the diffusion equation in the fuel region, the net number of neutrons in this

region is equal to the neutrons produced minus those lost by absorption or leakage and the one dimensional differential equation for the flux distribution in the unsteady state can be written as,¹

$$D_1 \nabla^2 \phi - \Sigma_a \phi + k \Sigma_a \phi = \frac{\partial n}{\partial t} \quad (1)$$

This is the equation of continuity (8) where

$$D_1 \nabla^2 \phi = D_1 \frac{\partial^2 \phi}{\partial x^2} = \text{leakage term} \quad (2)$$

$$- \Sigma_a \phi = \text{absorption term} \quad (3)$$

$$k \Sigma_a \phi = \text{a production term} \quad (4)$$

and $\frac{\partial n}{\partial t} = \frac{1}{v} \frac{\partial \phi}{\partial t}$, since $\phi = nv$ (8) and v is con-

sidered constant. Equation (1) simplifies to

$$\frac{\partial^2 \phi}{\partial x^2} + B^2 \phi = \frac{1}{D_1 v} \frac{\partial \phi}{\partial t} \quad (5)$$

Equation (5) is the characteristic equation for the fuel regions of the reactor. The diffusion equation is the same in the graphite regions, except for the omission of the source term. The diffusion equation for the nonmultiplying graphite regions is $D_2 \frac{\partial^2 \phi}{\partial x^2} - \Sigma_a \phi = \frac{1}{v} \frac{\partial \phi}{\partial t}$ (6)

¹A list of symbols and definitions used in all expressions is given in the Appendix.

Simplification of equation (6) supplies the characteristic equation for the nonmultiplying graphite region

$$\rho_2 \frac{\partial^2 \phi}{\partial x^2} - \Sigma_a \phi = \frac{1}{V} \frac{\partial \phi}{\partial t} \quad (7)$$

$$\frac{\partial^2 \phi}{\partial x^2} - \frac{1}{L_T^2} \phi = \frac{1}{V \rho_2} \frac{\partial \phi}{\partial t} \quad (8)$$

Equations (5) and (8) are descriptive of the one-dimensional unsteady state flux distribution in the two regions of consideration in the reactor. Though the fission mechanism is stochastic in nature, equation (5) is considered valid throughout each core region and equation (8) is valid throughout each graphite region.

The development of a heat balance in a volume element containing a heat source provides an initial step in the derivation of the characteristic equations of the thermal model. From the law of conservation of energy, the net flow out of heat energy must equal the flow of heat energy into the volume plus the heat energy generated within the volume minus the heat energy lost within the volume; this difference is the change in the internal energy of the volume element. Figure 3 illustrates heat conduction in a

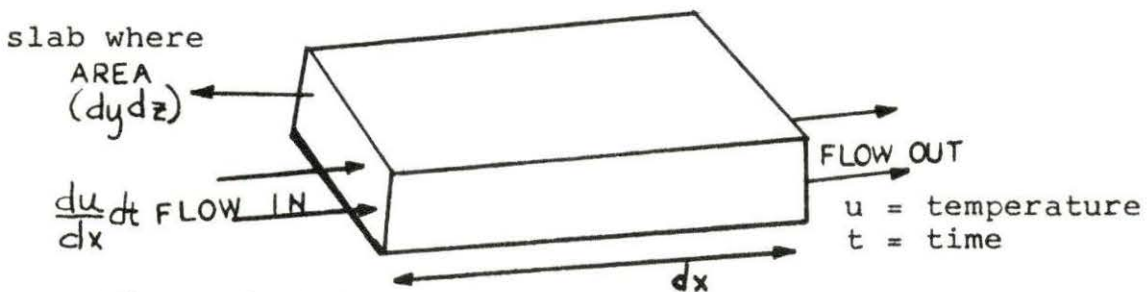


Figure 3. Volume element with a heat source

The amount of heat in the volume in the x direction is given by $-k \frac{du}{dx} dt (dy dz)$. The thermal conductivity k is basi-

cally a transport property of the medium. The temperature gradient $\frac{du}{dx}$ describes the distance rate change of temper-

ature. Finally dt is the change in time and dy dz is the flow-in area. Since the (flow-in, conduction in x direc-

$$\text{tion}) = -k \frac{du}{dx} dt dy dz \quad (9)$$

and the (flow-out, conduction in x direction) =

$$-k \frac{d}{dx} \left(u + \frac{du}{dx} dx \right) dt dy dz, \quad (10)$$

the net flow-out in the x direction = flow-in - flow-out,

or (net flow-out, in the x direction) =

$$\begin{aligned} & -k \frac{du}{dx} dt dy dz - \left[-k \frac{d}{dx} \left(u + \frac{du}{dx} dx \right) dt dy dz \right] \\ & = -k \frac{\partial^2 u}{\partial x^2} dx dy dz dt \end{aligned} \quad (11)$$

similarly it can be shown that

(net flow in y direction) =

$$-k \frac{\partial^2 u}{\partial y^2} dy dx dz dt \quad (12)$$

and

(net flow in z direction) =

$$-k \frac{\partial^2 u}{\partial z^2} dy dz dx dt \quad (13)$$

Thus, the total heat loss is the sum of the heat losses in

the three directions.

$$-\left(k \frac{\partial^2 u}{\partial x^2} dx dy dz dt + k \frac{\partial^2 u}{\partial y^2} dy dz dx dt + k \frac{\partial^2 u}{\partial z^2} dz dy dx dt\right) \\ = -k (\nabla^2 u) dx dy dz dt \quad (14)$$

$$\text{The total heat loss} = -k (\nabla^2 u) dx dy dz dt \quad (15)$$

The next point to be considered is the heat lost within the element volume in order to raise its temperature; in other words the heat stored is to be considered.

$$\text{Heat stored} = c\rho \frac{\partial u}{\partial t} dx dy dz dt \quad (16)$$

The specific heat gives the quantity of heat required to raise the temperature of a body per unit mass by one degree.

Thus, $c\rho$ is the heat required to raise the temperature of a unit volume one degree. So, $c\rho \frac{\partial u}{\partial t} dx dy dz dt$ accounts for

the heat stored. Since this volume element contains a heat source, P can be defined as the amount of heat generated per unit volume per unit time. The total heat generated becomes $P dx dy dz dt$. Now, the heat balance can be written as the heat stored = heat generated - heat lost.

$$c\rho \frac{\partial u}{\partial t} dx dy dz dt = \\ P dx dy dz dt + k (\nabla^2 u) dx dy dz dt \quad (17)$$

$$\text{This reduces to} \quad k (\nabla^2 u) + P = c\rho \frac{\partial u}{\partial t} \quad (18)$$

or

$$\nabla^2 U + \frac{P}{R} = \frac{c\rho}{R} \frac{\partial U}{\partial t} \quad (19)$$

If heat is generated proportional to temperature an equation

$P = \alpha U$ can be written. Now equation (19) can be re-written

$$\nabla^2 U + \frac{\alpha U}{R} = \frac{c\rho}{R} \frac{\partial U}{\partial t} \quad (20)$$

Equation (20) is the general expression for the temperature distribution for unsteady state conduction in the case of a source presence.

Although the reactor characteristic equations are written to describe a slab reactor, it is convenient to use a cylindrical rod geometry for the model.

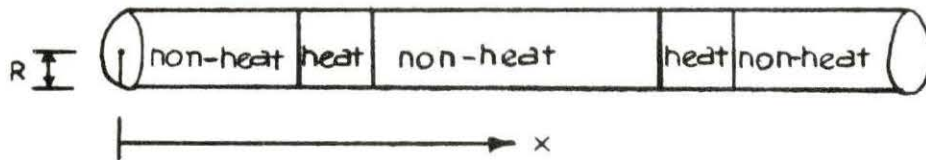


Figure 4. Sketch of thermal model

For a cylindrical rod region with a heat source, equation

(20) becomes

$$\frac{\partial^2 U_F}{\partial x_M^2} + \frac{\partial^2 U_F}{\partial r^2} + \frac{1}{r} \frac{\partial U_F}{\partial r} + \frac{1}{r^2} \frac{\partial^2 U_F}{\partial \theta^2} + \frac{\alpha U_F}{R_1} = \frac{c_1 \rho_1}{R_1} \frac{\partial U_F}{\partial t_M} \quad (21)$$

For a non-heat source region, equation (20) becomes

$$\frac{\partial^2 U_G}{\partial r^2} + \frac{1}{r} \frac{\partial U_G}{\partial r} + \frac{1}{r^2} \frac{\partial^2 U_G}{\partial \theta^2} + \frac{\partial^2 U_G}{\partial x_M^2} = \frac{c_2 \rho_2}{R_2} \frac{\partial U_G}{\partial t_M} \quad (22)$$

From symmetry considerations the angular temperature variations can be neglected and the terms $\frac{1}{r^2} \frac{\partial^2 U_G}{\partial \theta^2}$ and $\frac{1}{r^2} \frac{\partial^2 U_F}{\partial \theta^2}$ are dropped from the equations. The terms $\frac{\partial^2 U_G}{\partial r^2}$ and

$\frac{\partial^2 U_F}{\partial r^2}$ are also dropped by the assumption of linear radial change in temperature. From Newton's law of cooling (7)

$$q = -k A \left. \frac{\partial U}{\partial r} \right|_{r=R} = h A (U - U_a) \quad (23)$$

Equation (23) reduces to the following expression,

$$\left. \frac{\partial U}{\partial r} \right|_{r=R} = \frac{h}{-k} [U(R, x_M, t_M) - U_a]. \quad (24)$$

This means that the term $\frac{1}{R} \left. \frac{\partial U}{\partial r} \right|_{r=R}$ becomes

$$-\frac{h}{Rk} [U(R, x_M, t_M) - U_a].$$

Now equations (21) and (22) can be re-

written as

$$-\frac{h_1}{R_1 R} [U_F(R, x_M, t_M) - U_a] + \frac{\partial^2 U_F(R, x_M, t_M)}{\partial x_M^2} + \frac{\alpha}{R_1} U_F(R, x_M, t_M) = \frac{c_1 \rho_1}{R_1} \frac{\partial U_F(R, x_M, t_M)}{\partial t_M}$$

and

$$-\frac{h_2}{R_2 R} [U_G(R, x_M, t_M) - U_a] + \frac{\partial^2 U_G(R, x_M, t_M)}{\partial x_M^2} = \frac{c_2 \rho_2}{R_2} \frac{\partial U_G(R, x_M, t_M)}{\partial t_M}$$

The following functions can now be defined as

$$U_F' = U_F(R, x_M, t_M) - U_a$$

and

$$U_G' = U_G(R, x_M, t_M) - U_a.$$

since

$$\frac{\partial^2 U_F'}{\partial x_M^2} = \frac{\partial^2 [U_F(R, x_M, t_M) - U_a]}{\partial x_M^2} = \frac{\partial^2 U_F(R, x_M, t_M)}{\partial x_M^2}$$

$$\frac{\partial^2 U'_G}{\partial x_M^2} = \frac{\partial^2 [U_G(R, x_M, t_M) - U_a]}{\partial x_M^2} = \frac{\partial^2 U_G(R, x_M, t_M)}{\partial x_M^2}$$

and

$$\frac{\partial U'_F}{\partial t_M} = \frac{\partial [U_F(R, x_M, t_M) - U_a]}{\partial t_M} = \frac{\partial U_F}{\partial t_M}$$

$$\frac{\partial U'_G}{\partial t_M} = \frac{\partial [U_G(R, x_M, t_M) - U_a]}{\partial t_M} = \frac{\partial U_G}{\partial t_M}$$

equations (25) and (26) can be simplified.

$$\frac{\partial^2 U'_F(R, x_M, t_M)}{\partial x_M^2} + \left(\frac{\alpha}{R_1} - \frac{h_1}{R_1 R} \right) U'_F(R, x_M, t_M) = \frac{c_1 A}{R_1} \frac{\partial U'_F(R, x_M, t_M)}{\partial t_M} \quad (27)$$

$$\frac{\partial^2 U'_G(R, x_M, t_M)}{\partial x_M^2} - \frac{h_2}{R_2 R} U'_G(R, x_M, t_M) = \frac{c_2 \rho_2}{R_2} \frac{\partial U'_G(R, x_M, t_M)}{\partial t_M} \quad (28)$$

These equations are no longer effectively dependent on r ,

and it will be understood that $U'_F(R, x_M, t_M) = U'_F(x_M, t_M)$

and $U'_G(R, x_M, t_M) = U'_G(x_M, t_M)$. For convenience

these functions can be redefined so that $U'_F(x_M, t_M) =$

$U_F(x_M, t_M)$ and $U'_G(x_M, t_M) = U_G(x_M, t_M)$.

Therefore the following equations are approximately correct for the model one-dimensional case. Equation (29) is the characteristic equation for the source regions of the thermal analog.

$$\frac{\partial^2 U_F(x_M, t_M)}{\partial x_M^2} + \left[\frac{\alpha}{k_1} - \frac{h_1}{k_1 R} \right] U_F(x_M, t_M) = \frac{c_1 \rho_1}{k_1} \frac{\partial U_F(x_M, t_M)}{\partial t_M} \quad (29)$$

Equation (30) is the characteristic equation for the non-source regions of the thermal analog.

$$\frac{\partial^2 U_G(x_M, t_M)}{\partial x_M^2} - \frac{h_2}{k_2 R} U_G(x_M, t_M) = \frac{c_2 \rho_2}{k_2} \frac{\partial U_G(x_M, t_M)}{\partial t_M} \quad (30)$$

In summary, the four characteristic equations for the reactor prototype and the model are as follows:

Reactor

Source region:

$$\frac{\partial^2 \phi_F}{\partial x^2} + B^2 \phi_F = \frac{1}{\theta_1 V} \frac{\partial \phi_F}{\partial t} \quad (31)$$

Non-source region:

$$\frac{\partial^2 \phi_G}{\partial x^2} - \frac{1}{L_T^2} \phi_G = \frac{1}{\theta_2 V} \frac{\partial \phi_G}{\partial t} \quad (32)$$

Thermal Analog

Source region:

$$\frac{\partial^2 U_F}{\partial x_M^2} + \left(\frac{\alpha}{k_1} - \frac{h_1}{k_1 R} \right) U_F = \frac{c_1 \rho_1}{k_1} \frac{\partial U_F}{\partial t_M} \quad (33)$$

Non-source region:

$$\frac{\partial^2 U_G}{\partial x_M^2} - \frac{h_2}{k_2 R} U_G = \frac{c_2 \rho_2}{k_2} \frac{\partial U_G}{\partial t_M} \quad (34)$$

Establishment of the Relationship Between the
Characteristic Equations

The characteristic equations display similarities. Equations (31) and (33) as a pair and equations (32) and (34) as another pair may be related through the use of arbitrary constants. In order to consider equations (31) and (33) as related through the use of arbitrary constants, the following are defined:

$$\phi = n u \quad (35)$$

$$X = n_1 x_M \quad (36)$$

$$t = n_2 t_M \quad (37)$$

The subscripts M refer to the model; n , n_1 , and n_2 are arbitrary, dimensionless constants in the case of n_1 and n_2 . The quantity n necessarily must have dimensions; Now, the neutron diffusion equation (31) can be expressed in terms of the model and arbitrary constants.

$$\frac{n}{n_1^2} \frac{\partial^2 u}{\partial x_M^2} + B^2 n u = \frac{1}{D_{1v}} \frac{n}{n_2} \frac{\partial u}{\partial t_M} \quad (38)$$

This equation reduces to

$$\frac{\partial^2 u}{\partial x_M^2} + n_1^2 B^2 u = \frac{1}{D_{1v}} \frac{n_1^2}{n_2} \frac{\partial u}{\partial t_M} \quad (39)$$

Equation (39) will be analogous to equation (29) if,

$$\frac{\alpha}{K_1} - \frac{h_1}{K_{1R}} = n_1^2 B^2 \quad (40)$$

and

$$\frac{c_1 \rho_1}{k_1} = \frac{n_1^2}{n_2} \frac{1}{\theta_1 v} \quad (41)$$

A similar development can be used with equations (32) and (34). Since the proportionality between time and distance in each pair of characteristic equations is the same, the proportionality between the flux and the temperature should also be the same. In a manner similar to that used just previously, it can be shown that the same substitutions hold true. Now equation (32) can be written in terms of the arbitrary constants and model variables,

$$\frac{n}{n_1^2} \frac{\partial^2 u}{\partial x_M^2} - \frac{1}{L_T^2} n u = \frac{1}{\theta_2 v} \frac{n}{n_2} \frac{\partial u}{\partial t_M} \quad (42)$$

which reduces to

$$\frac{\partial^2 u}{\partial x_M^2} - \frac{n_1^2}{L_T^2} u = \frac{n_1^2}{\theta_2 n_2 v} \frac{\partial u}{\partial t_M} \quad (43)$$

This equation will be analogous to equation (34) if the following relationships are made:

$$\frac{h_2}{k_2 R} = \frac{n_1^2}{L_T^2} \quad (44)$$

and

$$\frac{c_2 \rho_2}{k_2} = \frac{n_1^2}{n_2} \frac{1}{\theta_2 v} \quad (45)$$

In summary, equations (31) and (33) are analogous if,

$$\frac{\alpha}{k_1} - \frac{h_1}{k_1 R} = n_1^2 B^2 \quad (40)$$

$$\frac{c_1 \rho_1}{k_1} = \frac{n_1^2}{n} \frac{1}{\sqrt{D_1}} \quad (41)$$

Equations (32) and (34) are analogous if,

$$\frac{h_2}{k_2 R} = \frac{n_1^2}{L_T^2} \quad (44)$$

$$\frac{c_2 \rho_2}{k_2} = \frac{n_1^2}{D_2 n_2 V} \quad (45)$$

ϕ_F and ϕ_G refer to the neutron flux in the system and the subscripts refer to the particular region of concern; the same is true for the analogous temperatures in the model.

Boundary Conditions Considerations

With the necessary relationships between the characteristic equations developed, the boundary conditions should be observed next. The diagram of the two core reactor indicates that equation (31) refers to regions 2 and 4, and equation (32) refers to regions 1, 3, and 5.

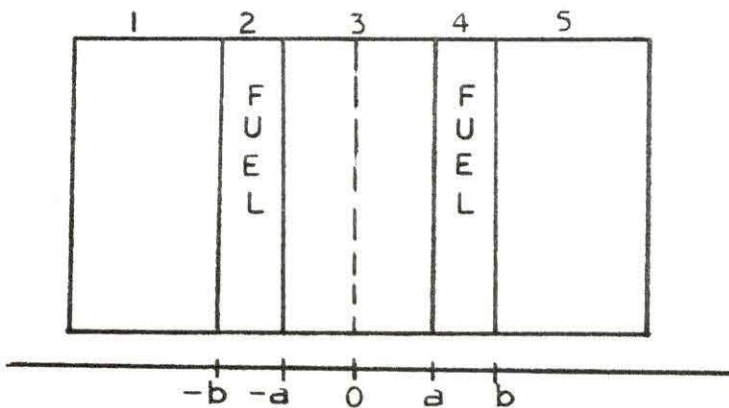


Figure 5. Boundaries of a two core reactor

Now from the diagram the boundary conditions can be written.

(a) Since the flux must be continuous across the bound-

ary between two different media (8),

$$\phi_F \Big|_{x=\pm a, \pm b} = \phi_G \Big|_{x=\pm a, \pm b} \quad (46)$$

(b) Since there can be no accumulation of neutrons at an interface, the net number of neutrons leaving one medium per second per unit area must equal the number of neutrons that enter the other medium per second per unit area (8). From Fick's law (8) this boundary condition may be expressed as

$$D_1 \frac{d\phi_F}{dx} \Big|_{x=\pm a, \pm b} = D_2 \frac{d\phi_G}{dx} \Big|_{x=\pm a, \pm b} \quad (47)$$

(c) To establish a time reference the fluxes in both regions of fuel and reflector are assumed to be constant for particular values of x and at time zero.

$$\phi_F = \text{CONSTANT} \quad -b < x < -a, \quad a < x < b, \quad t=0$$

$$\phi_G = \text{CONSTANT} \quad -a < x < a, \quad t=0$$

Next is the consideration of the boundary conditions of the thermal analog.

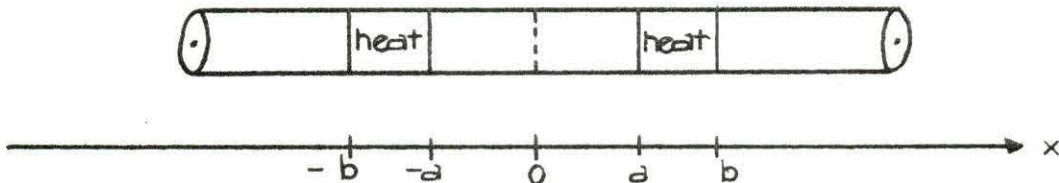


Figure 6. Boundaries of thermal model

From the figure the boundary conditions can be written as follows:

(a') The temperature must be the same across the inter-

face of the two different media.

$$U_F \Big|_{x=\pm a, \pm b} = U_G \Big|_{x=\pm a, \pm b} \quad (48)$$

(b') Since there can be no heat accumulation at the interfaces, the flow of heat leaving one medium per second per unit area must equal that entering the other medium per second per unit area. From Fourier's law of heat conduction

$$k_1 \frac{dU_F}{dx} \Big|_{x=\pm a, \pm b} = k_2 \frac{dU_G}{dx} \Big|_{x=\pm a, \pm b} \quad (49)$$

(c') The temperatures in the regions of heat and non-heat sources are considered constant for particular values of x and time zero, in order to establish a time reference.

$$U_F = \text{CONSTANT} \quad -b < x < -a, a < x < b, t=0 \quad (50)$$

$$U_G = \text{CONSTANT} \quad -a < x < a, t=0 \quad (51)$$

The model boundary conditions are derivable from the reactor boundary conditions by making the necessary substitutions:

$$\phi_F = n U_F \quad x = n_1 x_M$$

$$\phi_G = n U_G \quad t = n_2 t_M$$

$$\frac{d\phi_F}{dx} = \frac{n}{n_1} \frac{dU_F}{dx_M}$$

$$\frac{d\phi_G}{dx} = \frac{n}{n_1} \frac{dU_G}{dx_M}$$

From equation (41)

$$\frac{c_1 \rho_1}{k_1} = \frac{n_1^2}{n_2} \frac{1}{D_1 v}$$

and solving for D_1 results in $D_1 = \frac{k_1 n_1^2}{n_2 c_1 \rho_1 v}$ (52)

for heat source regions. From equation (45), the diffusion coefficient for the non-heat source region is given by

$$D_2 = \frac{k_2 n_1^2}{n_2 c_2 \rho_2 v} \cdot \quad (53)$$

With these substitutions and the fact that v is assumed to be constant in any medium, the reactor boundary conditions may be rewritten as follows:

$$(a') \quad n U_F \Big|_{x=\pm a, \pm b} = n U_G \Big|_{x=\pm a, \pm b} \quad \text{which reduces to}$$

$$U_F \Big|_{x=\pm a, \pm b} = U_G \Big|_{x=\pm a, \pm b}$$

(b')

$$\frac{k_1 n_1^2}{c_1 \rho_1 n_2 v} \frac{n}{n_1} \frac{dU_F}{dx_M} \Big|_{x=\pm a, \pm b} = \frac{k_2}{c_2 \rho_2 n_2 v} \frac{n}{n_1} \frac{dU_G}{dx_M} \Big|_{x=\pm a, \pm b} \quad (54)$$

which reduces to

$$\frac{k_1}{c_1 \rho_1} \frac{dU_F}{dx_M} \Big|_{x=\pm a, \pm b} = \frac{k_2}{c_2 \rho_2} \frac{dU_G}{dx_M} \Big|_{x=\pm a, \pm b}$$

From Fourier's law

$$k_1 \frac{dU_F}{dx_M} \Big|_{x=\pm a, \pm b} = k_2 \frac{dU_G}{dx_M} \Big|_{x=\pm a, \pm b} \cdot$$

This establishes the condition that

$$k_1 \frac{dU_F}{dx_M} \Big|_{x=\pm a, \pm b} = k_2 \frac{dU_G}{dx_M} \Big|_{x=\pm a, \pm b} \quad (55)$$

from which $c_1 \rho_1 = c_2 \rho_2$. The proper materials selection can satisfy this condition.

(c') Finally, the third reactor boundary condition can be rewritten in terms of the constants and model terms which yield the same boundary condition as expressed in condition (c') of the thermal analog.

In summary, the boundary conditions of the reactor can be put into terms of the analog conditions, providing that the materials selected for the thermal analog comply with the following design conditions:

$$\frac{\alpha}{k_1} - \frac{h_1}{k_1 R} = \eta_1^2 B^2 \quad (40)$$

$$\frac{c_1 \rho_1}{k_1} = \frac{\eta_1^2}{\eta_2} \frac{1}{A_1 V} \quad (41)$$

$$\frac{h_2}{k_2 R} = \frac{\eta_1^2}{L_T^2} \quad (44)$$

$$\frac{c_2 \rho_2}{k_2} = \frac{\eta_1^2}{\eta_2} \frac{1}{A_2 V} \quad (45)$$

$$U_F \Big|_{x=\pm a, \pm b} = U_G \Big|_{x=\pm a, \pm b} \quad (54)$$

$$k_1 \frac{dU_F}{dx_M} \Big|_{x=\pm a, \pm b} = k_2 \frac{dU_G}{dx_M} \Big|_{x=\pm a, \pm b} \quad (55)$$

$$c_1 \rho_1 = c_2 \rho_2$$

ACTUAL MODEL DESIGN

Materials Selection

The first step in the design of the model is selecting two materials for the thermal analog, materials which can be related to graphite and fuel regions of the two core UTR-10 Reactor. From previous work (9) the one-group values of the diffusion coefficient of the graphite and fuel regions are

$$D_1 = 0.121 \text{ CM} \quad \text{fuel region and}$$

$$D_2 = 0.843 \text{ CM} \quad \text{graphite region}$$

From the summary definition requirements, a ratio of $\frac{D_1}{D_2}$ must satisfy the following conditions, $\frac{D_1}{D_2} = \frac{k_1}{k_2} \Rightarrow c_1 \rho_1 = c_2 \rho_2$

The values of D_1 and D_2 establish the requirements imposed on the relative conductivities of the materials for the source and non-source regions. $k_1 = 0.144 k_2$

Table 1. Determination of source and non-source materials

Material	Thermal Conductivity of Material, K cal/sec cm °C	0.144 K cal/sec cm °C
Iron	0.151	0.022
Copper	1.043	0.1502
Aluminum	0.490	0.0706
Lead	0.082	0.012
Steel	0.107	0.0154

From the tabulated calculations it is ascertained that the best choice of materials is for heat source sections of iron and non-heat source sections of copper. This means that k_1 has the value 0.151 cal/cm sec °C for the iron selection and k_2 has the value 1.043 cal/cm sec °C for the copper selection. The condition that $c_1 \rho_1 = c_2 \rho_2$ must also hold. Thus at temperatures of consideration (limit of 167 °C), $C_{cu} \rho_{cu} \approx C_{Fe} \rho_{Fe}$ or 0.090246 cal/cm³ °C \approx 0.091104 cal/cm³ °C. These values are the best achievable and compare well with the definition requirement. Therefore, iron and copper are suitable choices. The materials are easily worked, permit good contacts at interfaces, and are relatively inexpensive.

Determination of Desirable Design Parameters

With the materials selected considerations can be given to the other design features. Relationships (40), (41), (44), and (45) are most important to the design conditions. They represent four linear equations with four unknown quantities n_1^2 , n_2 , α , and R to be determined. If $\alpha = x_1$, $n_1^2 = x_2$, $n_2 = x_3$, $\frac{1}{R} = x_4$ then these four equations may be rewritten as follows,

$$\frac{x_1}{R_1} - \frac{h_1 x_4}{R_1} - x_2 B^2 = 0 \quad (56)$$

$$\frac{c_1 \rho_1}{R_1} x_3 - \frac{x_2}{B_2 v} = 0 \quad (57)$$

$$\frac{x_2^2}{L_T^2} - x_4 \frac{h^2}{R_2} = 0 \quad (58)$$

$$\frac{x_2}{B_2 V} - \frac{C_2 \rho_2}{R^2} x_3 = 0 \quad (59)$$

It can be shown that the solution of this system of equations is

$$x_4 = \frac{1}{R} \quad (60)$$

$$\alpha = \frac{h_1 R_2 + h_2 k_1 L_T^2 B^2}{R R_2} \quad (61)$$

$$n_1^2 = \frac{h_2 L_T^2}{R_2 R} \quad (62)$$

$$n_2 = \frac{h_2 L_T^2 R_1}{R_2 R B_1 V C_1 \rho_1} \quad (63)$$

The unknown quantities can now be determined by substituting in the formulas the known values of all the terms, except those for the film coefficient and the radius of the rod.

Table 2. Properties of iron and copper (6)
(for temperatures of consideration)

Material	Density, ρ (gm/cm ³)	Specific Heat, c (cal/gm °C)	Thermal Conductivity, k (cal/sec cm °C)
Iron	7.8	0.1168	0.151
Copper	8.9	0.1014	1.043

Table 3. Properties of reactor core and materials
(for one-group theory) (9)

Diffusion Coefficients, cm		Macroscopic, cm ⁻¹ Cross Section		No. of Neut/Fission	L _T ² , cm ²	B ² , cm ⁻²
D ₁	D ₂	Σ _a	Σ _f	ν		
0.121	0.843	0.0908	0.0502	2.44	9.29	0.262

With these values of the material properties, B, and L, equations (61), (62), and (63) can be rewritten as

$$\alpha = \left[\left(\frac{h_1}{R} \right) + 0.353 \left(\frac{h_2}{R} \right) \right] \text{ cal/sec cm}^3 \text{ } ^\circ\text{C} \quad (61)$$

$$\eta_1 = 2.985 \left(\frac{h_2}{R} \right)^{1/2} \quad (62)$$

$$\eta_2 = 5.56 \times 10^{-5} \left(\frac{h_2}{R} \right) \quad (63)$$

Before suitable values of h and R are determined, the limitations on the design of the model must be considered. The model size is determined from the given reactor size and limitations of laboratory space. From experimental work further limitation on the model size is the ability to detect a heat pulse at certain distances from a heat pulsing device on one end of the rod. Model frequencies are limited by the thermal conductivity of the material. A limiting factor on the diameter of the rod is the size of the thermistors used in taking temperature readings. Size is also

an important consideration in the method of heating and controlling the model heat sources of iron. Finally, α (the proportionality constant between temperature and heat generated in the iron sources) must remain small to avoid the possibility of an unstable system.

Since the model frequencies can only be determined within the limits of the ability of iron or copper to conduct heat, and since the temperature-power proportionality constant depends heavily on the equipment available for producing power in the model heat source regions, the only design parameters left with a small but considerably better degree of latitude in selection are the dimensionless length scale, n_1 , and R , the radius of the rod. From experimental results of the best responses to temperature variations along the rod as a function of size, lengthwise distance from the pulse generator, thermistor size and locations, a radius of 0.317 cm was selected and an n_1 value of 15. In the reactor prototype the core regions are approximately 15 cm wide and the graphite coupling region between them 45 cm long. Thus from the similitude requirement that

$\chi = n_1 \chi_M$, the model iron heat source regions are each one cm long, with a radius of 0.317 cm. The copper coupling region between the iron cores is 3 cm long with a radius of 0.317 cm. The outer regions of copper are each arbitrarily selected to be approximately 10 cm long, with a radius of

0.317 cm. These measurements allow adequate space for a heat pulse driver section on one end of the rod and several thermistor locations on the other end. With values assigned to both R and n_1 , the solutions for the other design parameters can be evaluated, given the h_1 value. A good approximation for the film conductance due to free or natural convection of air at atmospheric pressure over horizontal rods less than a foot in diameter is given by the following restricted equation (3).

$$h = 0.23 \left(\frac{\Delta U}{2R} \right)^{\frac{1}{4}} \quad (64)$$

The temperature of the surrounding air is considered to be approximately room temperature, the constant 0.23 is approximated for experimental results, R is given in feet, and the temperature change is given in degrees fahrenheit. On the average, the temperature difference at most was found to be approximately 240° F in the non-heat source regions, and 280° F in the heat-source regions. Since the heat source section surface area is not as extensive as the non-heat source region, the conductance of heat to the surrounding medium in the non-heat source region is greater than that in the heat source region. From equation (64), the following values of h_1 and h_2 were determined: (with h_1 referring to the heat source region and the h_2 referring to the non-heat source region.)

$$h_1 = 3.33 \times 10^{-4} \quad \text{cal/sec cm}^2 \text{ } ^\circ\text{C}$$

$$h_2 = 3.19 \times 10^{-4} \quad \text{cal/sec cm}^2 \text{ } ^\circ\text{C}$$

With the values of h_1 , n_1 , and R specified the other design parameters determined for true model requirements can be evaluated as

$$\alpha = 14.05 \times 10^{-4} \quad \text{cal/sec cm}^3 \text{ } ^\circ\text{C}$$

$$\approx 1.06 \times 10^{-4} \quad \text{watts/}^\circ\text{k}$$

$$\eta_2 = 5.6 \times 10^{-8}$$

Equation (62) was first used to evaluate what true model requirements indicate the h_2 value to be. The value of h_2 obtained was $7.99 \text{ cal/sec cm}^2 \text{ } ^\circ\text{C}$, and it was used in the evaluation of equations (61) and (63). Obviously, the value of h_2 calculated from equation (64) is different from the value obtained from equation (62). This difference is a first indication that the model may not be a true one because the design conditions cannot all be satisfied. Another indication that this is not to be a true model can be seen from the value of the frequency or time scale value. From the relationship $\tau = \eta_2 \tau_M$, the model frequency is required to be 5.6×10^{-6} cps at the reactor sink frequency. Tests of the ability of iron or copper to respond to heat impulses at a specific frequency gave satisfactory response

at an average value of about 24.5 cps. In the laboratory tests the ability of iron or copper to conduct heat pulses at smaller cycle times was poor. This indicates that the calculated value of n_2 cannot be used effectively. To eliminate this problem necessitated considerations for a distorted model rather than a true one.

Direct resistance heating of the heat source regions was selected as being the most convenient method of heating considering the equipment available. Two washers were placed around the edges of the heat source regions as shown in figure 7. Extending from the washers were large leads. The leads were attached to current generators and at most 185 amperes of current was put into each of the iron source regions. Limitations on the thermistors required that no temperatures being measured by them exceed 300° F. It was also desirable to keep temperatures below the level where radiation of heat is negligible. With these limitations and considerations the three values of α selected for experimental use were

$$\alpha_1 = 4.4 \times 10^{-3} \quad \text{watts/}^\circ\text{k}$$

$$\alpha_2 = 2.85 \times 10^{-3} \quad \text{watts/}^\circ\text{k}$$

$$\alpha_3 = 1.59 \times 10^{-3} \quad \text{watts/}^\circ\text{k}$$

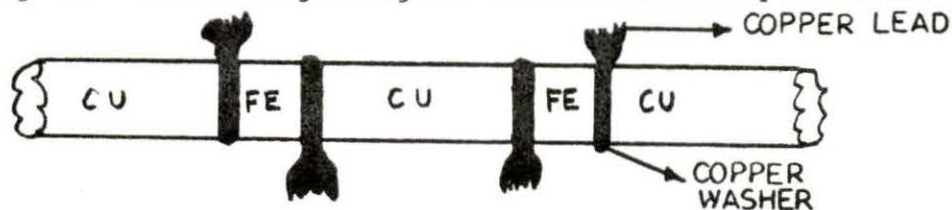
These values of α are different from the design values. After a value for the maximum current was chosen and after

calculating the resistance of iron from material properties and the area involved, a value for the power output was determined. Then from the relationship $P = \alpha U$ and using a maximum temperature of 300°F , the three values of α were selected within the experimental limitations.

In order to overcome the limitations discussed and still make an effective model study, the true model was finally rejected for one in which distortion was to occur in the frequency ranges and power output of the heat source regions. These proved to be fortunate in that the parameters affected were easily varied in the laboratory set-up, whereas distortion in the model size or geometry could require the actual construction of various models.

Model Construction

After all of the design conditions on the model were determined, the construction was done by the Machine Shop using the following diagram and listed requirements.



Washer width around iron source 0.2 cm
 Iron heat sources 1 cm long, 0.317 cm radius
 Copper between Iron 3 cm long, 0.317 cm radius
 Copper extreme regions 10 cm long, 0.317 cm radius

Figure 7. Drawing of model with dimensions given

All sections were silver soldered to provide the best contact. The copper leads to the heat source sections were made large enough to accommodate the thick wires carrying current of a hundred or more amperes. The large amounts of current supplied to the iron source regions were obtained from a transformer on one core and an ac arc welder on the other core. In order to control the power input to the source regions, voltmeters and ammeters continually monitored the amount of power in the source regions.

The last construction requirement was the heat pulse driver section. Heater wire wrapped around one electrically insulated end of the rod was connected to a dc power supply and the current pulsed by manual control. Of some concern was the selection of the insulation material which would give good electrical insulation, but allow the maximum heat conduction between the heater wire and the surface of the rod. After trial and error a combination of sauerisen insulator paste and torr seal paste gave the best results. An initial layer of sauerisen on the surface of the rod gave the necessary electrical insulation and proved resistant to the high temperatures involved in the experiment. An outer layer of torr seal cemented and held the layer of sauerisen firm to the rod. Two thin layers, one sauerisen and then torr seal were placed on the surface of the rod. The heater wire was then wrapped around this section of the

rod. Two more layers in the same order as the first two were placed on the outside of the heater wire. A final layer of asbestos paper was applied. The ends of the heater wire were then attached to a variable dc power supply and the current pulsed manually to achieve a sinusoidal variation temperature perturbation in the model system; as current flows in the heater wire it causes increases and decreases in temperatures according to the rise and fall of the current. The heat arises from resistance heating of the heater wire. This heat is then transmitted through conduction to the surface of the model, causing the perturbation in the model system.

The following diagram sketches the model set-up and on the following pages photographs show the actual laboratory set-up.

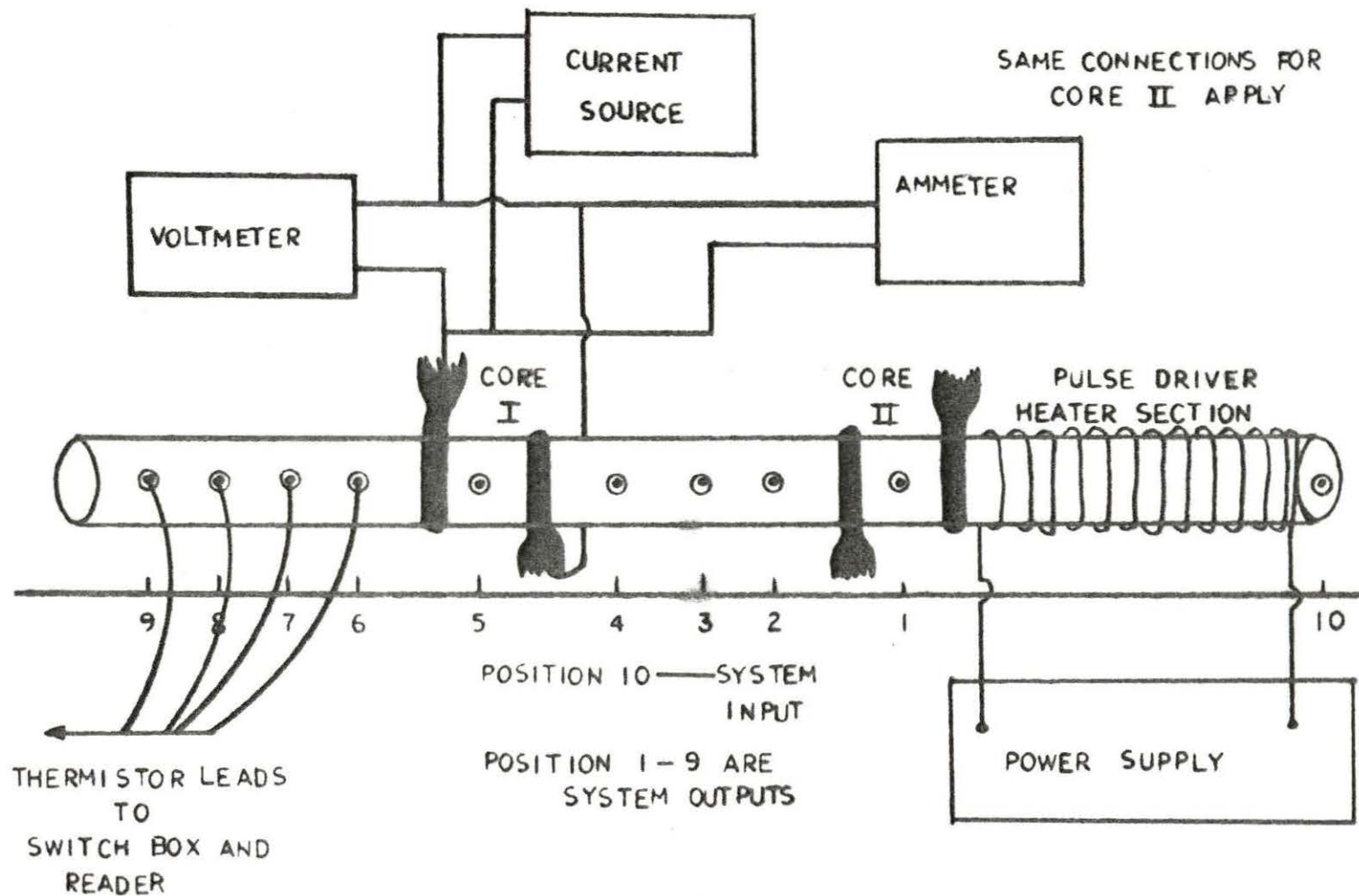


Figure 8. Sketch of model set-up

Figure 9. Close up view of the thermal model

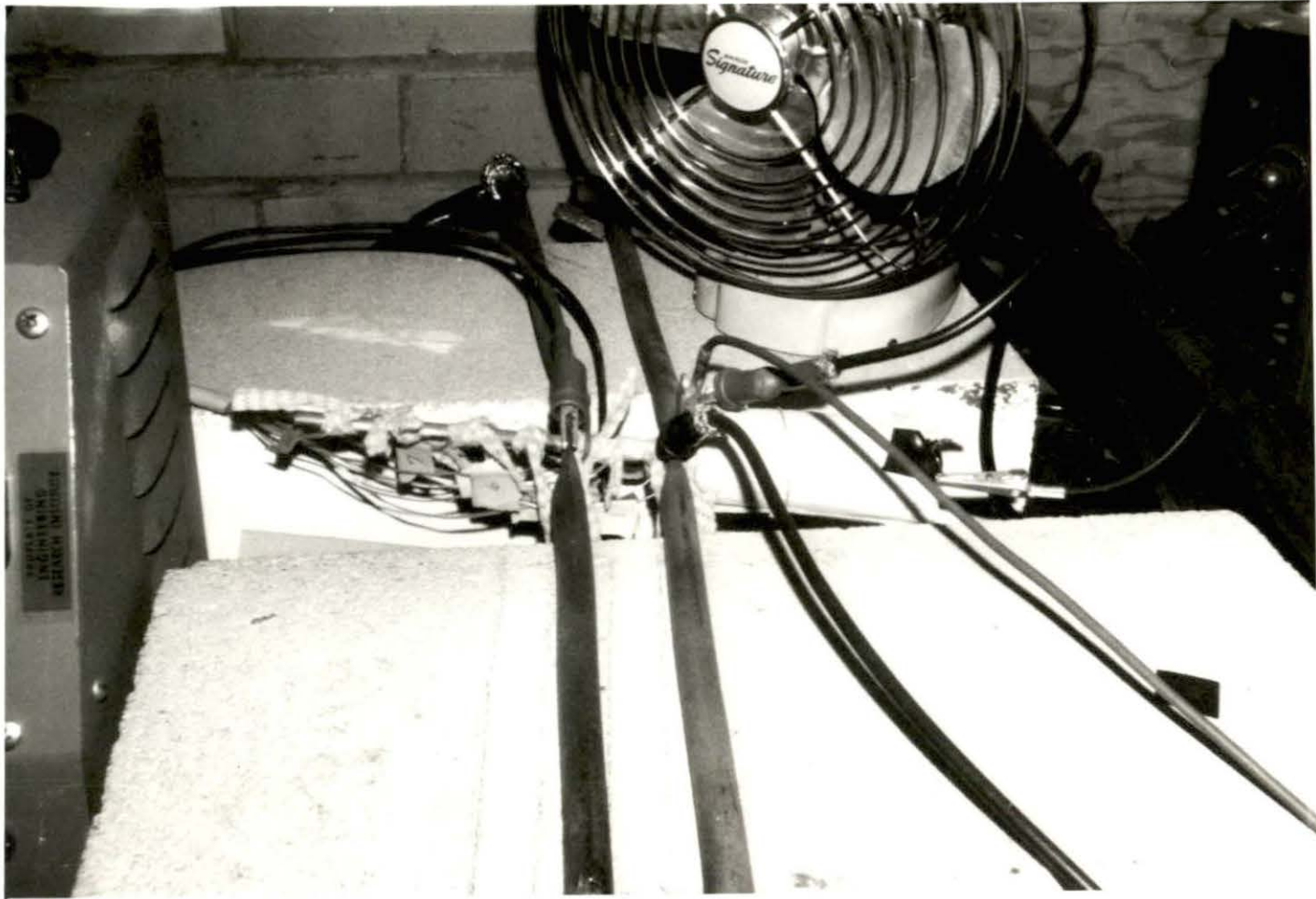


Figure 9. Close up view of the thermal model

Figure 10. Overall view of laboratory set up

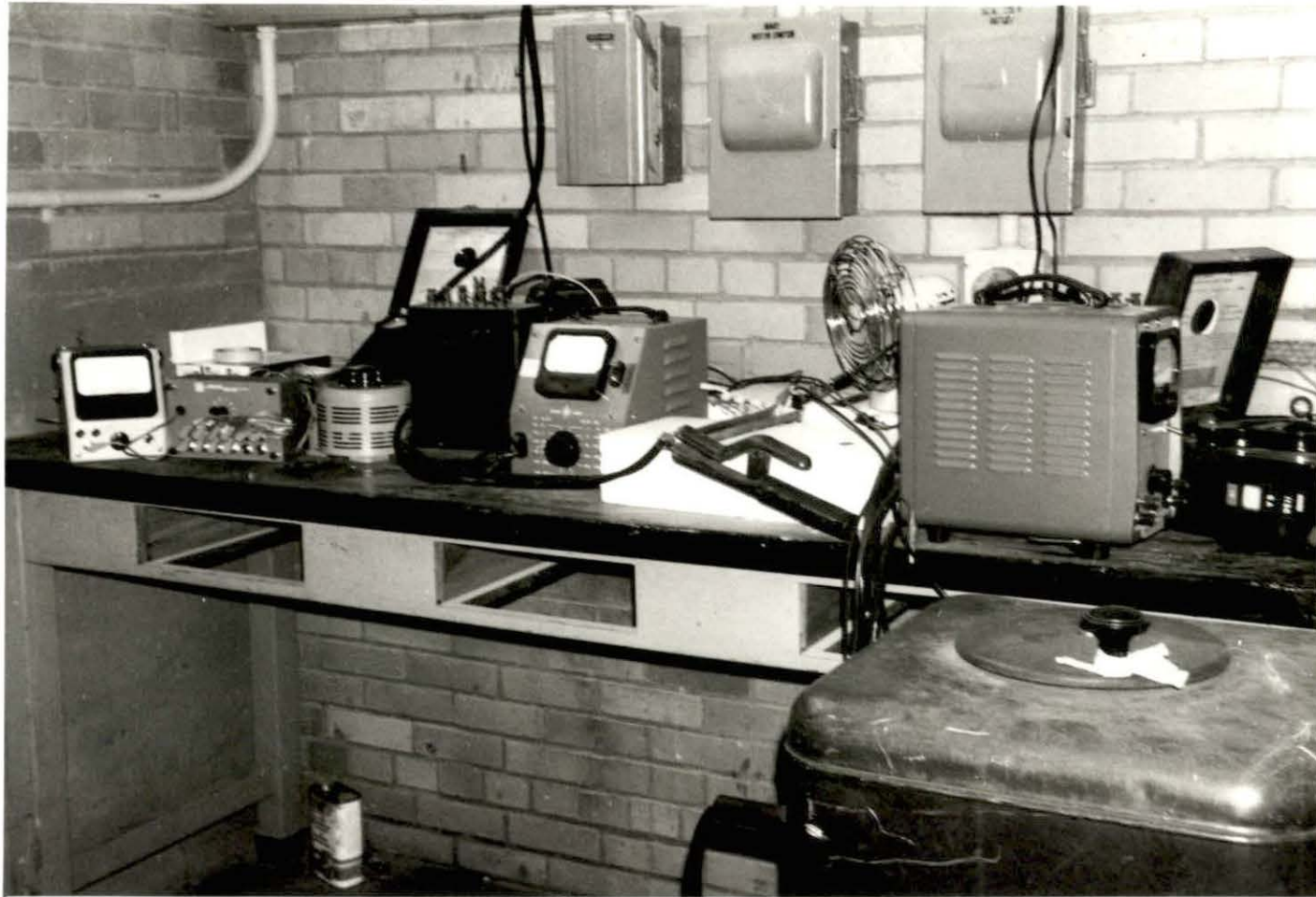


Figure 10. Overall view of laboratory set up

METHOD OF TAKING DATA AND
PLOTS OF RESULTS

With the described experimental set-up, collection of data required the efforts of three people. One person was needed to vary the dc power supply in order to give the current a half rectified sine wave variation. This affected the temperature pulse perturbation on the model system. With the use of a stopwatch and manual efforts, various frequencies within the experimental limits were achieved. Another person monitored the two cores in order to achieve the effect of proportional control of the heat source regions. A set of tables was prepared from which the temperature reading, voltage reading, current reading, and specified α value could be related as rapidly as possible to indicate how much the current to the heat source should be increased or decreased to achieve the proportional power-temperature control of $P = \alpha U$. This person worked as rapidly as possible continually monitoring the cores to ensure as much as possible the proportional behavior required between temperature and power. The third job included satisfying the initial conditions on the system before each trial run, and during the run, recording as rapidly as possible the temperature at the specific time at each of the ten thermistor locations. With the aid of a switch box and a stopwatch and practice, recordings of time and temperature for all ten positions were achieved on an average

of a minute. Each temperature reading taken at either of the two cores was called out to the person monitoring the cores. As rapidly as possible the tables were checked and the core power adjusted accordingly. At each frequency readings were taken for the duration of two cycles in the current sinusoidal variation. At the end of each run two fans were applied to the model to speed up its return to an initial steady state condition. Initial conditions involved making sure that the two cores were at the same fairly constant temperature level and the copper regions were also at a fairly constant temperature. Each time the cores were initially heated, a twenty-minute time period was allowed to pass to ensure small, almost no variations in temperatures. When this level was achieved the steady initial conditions on the system versus the thermistor locations on the rod show a temperature distribution as depicted in figure 12. This temperature distribution across the model positions for steady state shows good similarity to the spatial flux profile in the UTR-10 reactor for the equivalent steady condition. Since one-group theory has been assumed valid, the thermal flux distribution across the UTR-10 has the form shown in figure 11. This can be explained by the fact that in the coupling region, the thermal flux buildup results from the presence of neutrons contributed from both cores on either side. The same reasoning can

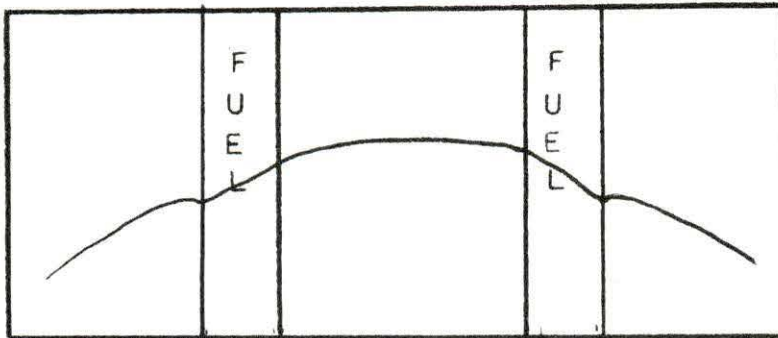


Figure 11. Flux distribution for the UTR-10

apply to the temperature buildup in the model coupling region, as a result of the presence of the two heat sources on either side. After the model was operated in initial conditions, simultaneously the pulsing with the dc power supply was started, the cores were monitored with changes in their power output controlled as continuously as possible, temperature and time recordings were made. Various pulse frequencies were tried. The response of the model to the sinusoidal input proved to be also sinusoidal but of different phase and magnitude. Figure 13 shows this behavior. From this plot the response at all thermistor locations indicates that the pulse was felt all along the rod. However, when shorter cycle times were used the pulse time was so fast until it was beyond the material response capability. Figure 14 shows that below a cycle time of one minute the pulse of heat was not felt along the rod nor even in the driver section. In actual practise all frequencies of any experimental value was obtained in the range of

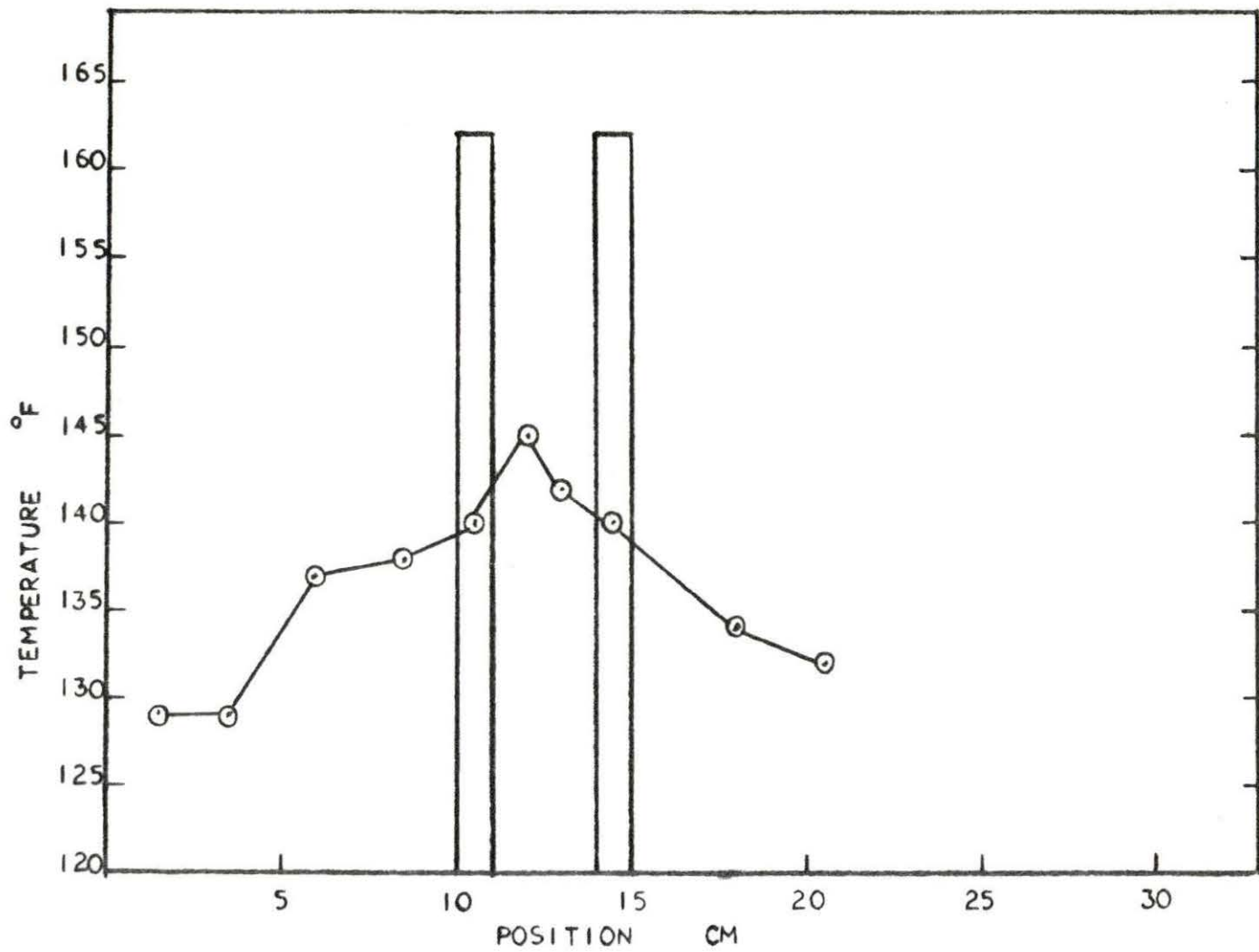


Figure 12. **Steady-state temperature distribution versus thermister location**

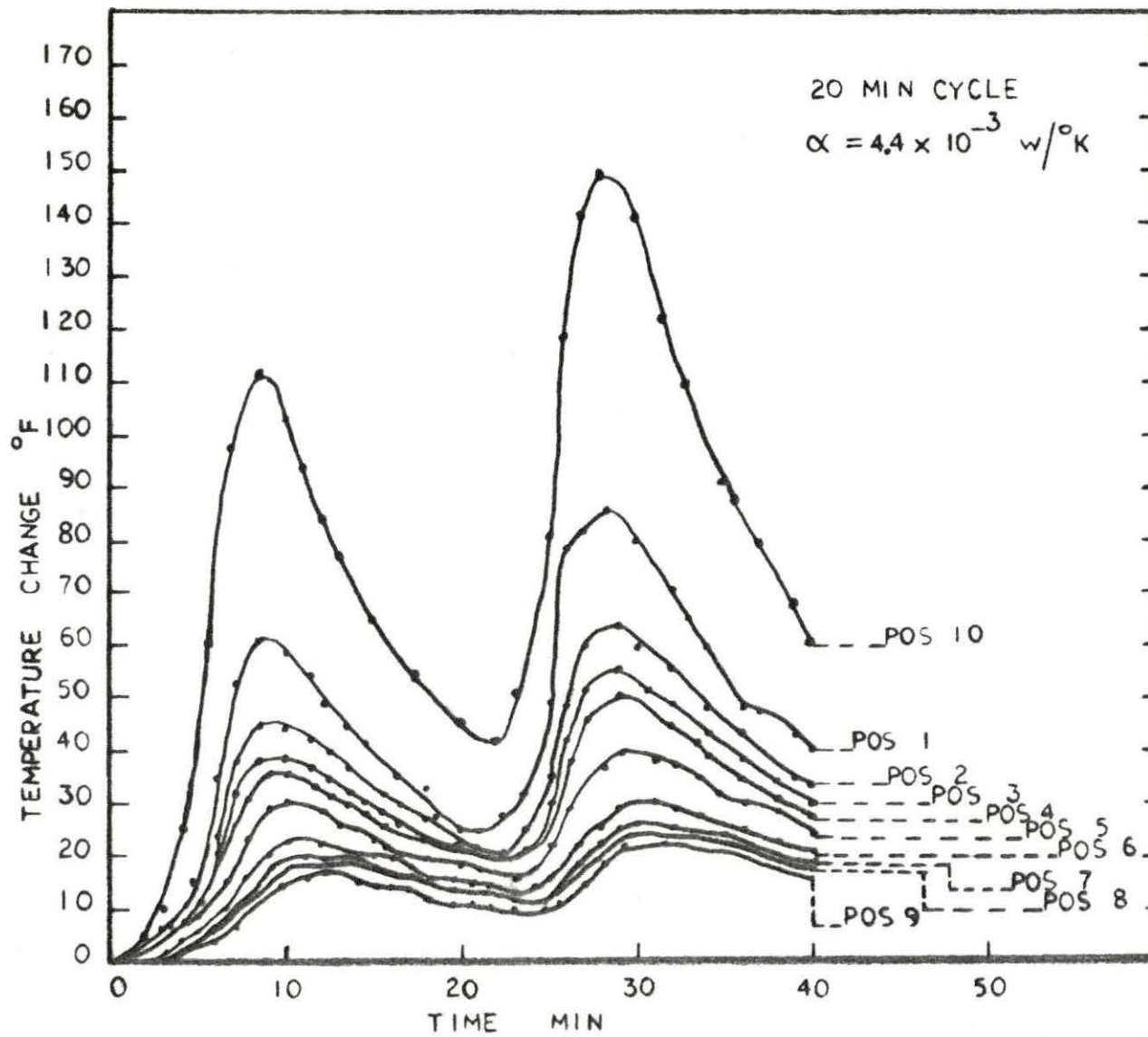


Figure 13. Temperature response versus time for each thermistor location

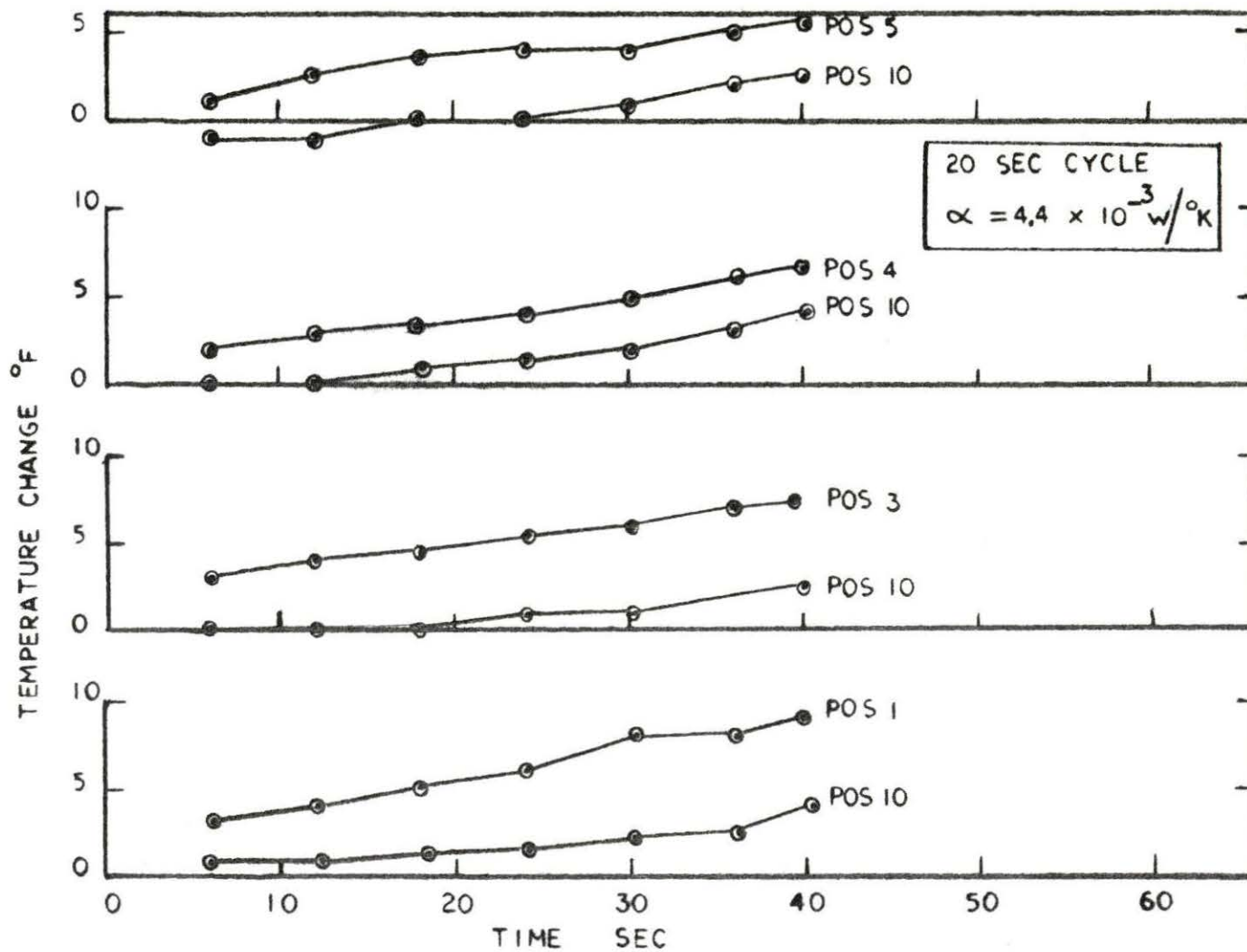


Figure 14. Temperature response versus time for several thermistor locations

cycle times above four minutes.

Of interest was a comparison of the model spatial temperature distribution during the pulsing action. This was done for two cases, namely the case where temperature-power ratio was neglected in the model core regions and the case where it was applied. Figures 15 and 16 depict these two conditions. From figure 15 it can be said that the temperature distribution shape does not vary in time during the pulsing, but varies in amplitude. This is also in accordance with the reactor prototype behavior. The usual assumption made in applying the point or space independent reactor kinetic equations is that the flux shows no time variation in shape. This assumption is necessary because some of the parameters involved in using the point kinetics equations can be evaluated only if the instantaneous flux shape is known. Another parallel shown here between the model and the prototype is the change in power level during the pulsing never allows the system to return to the initial power level.

From figure 16 the effect of temperature-power control in the model core regions produces little change in the overall temperature distribution shape. The greater drop between temperatures in core I and core II as opposed to the same difference in figure 15 is a result of using great-power in the heater section, thus increasing the heat pulse

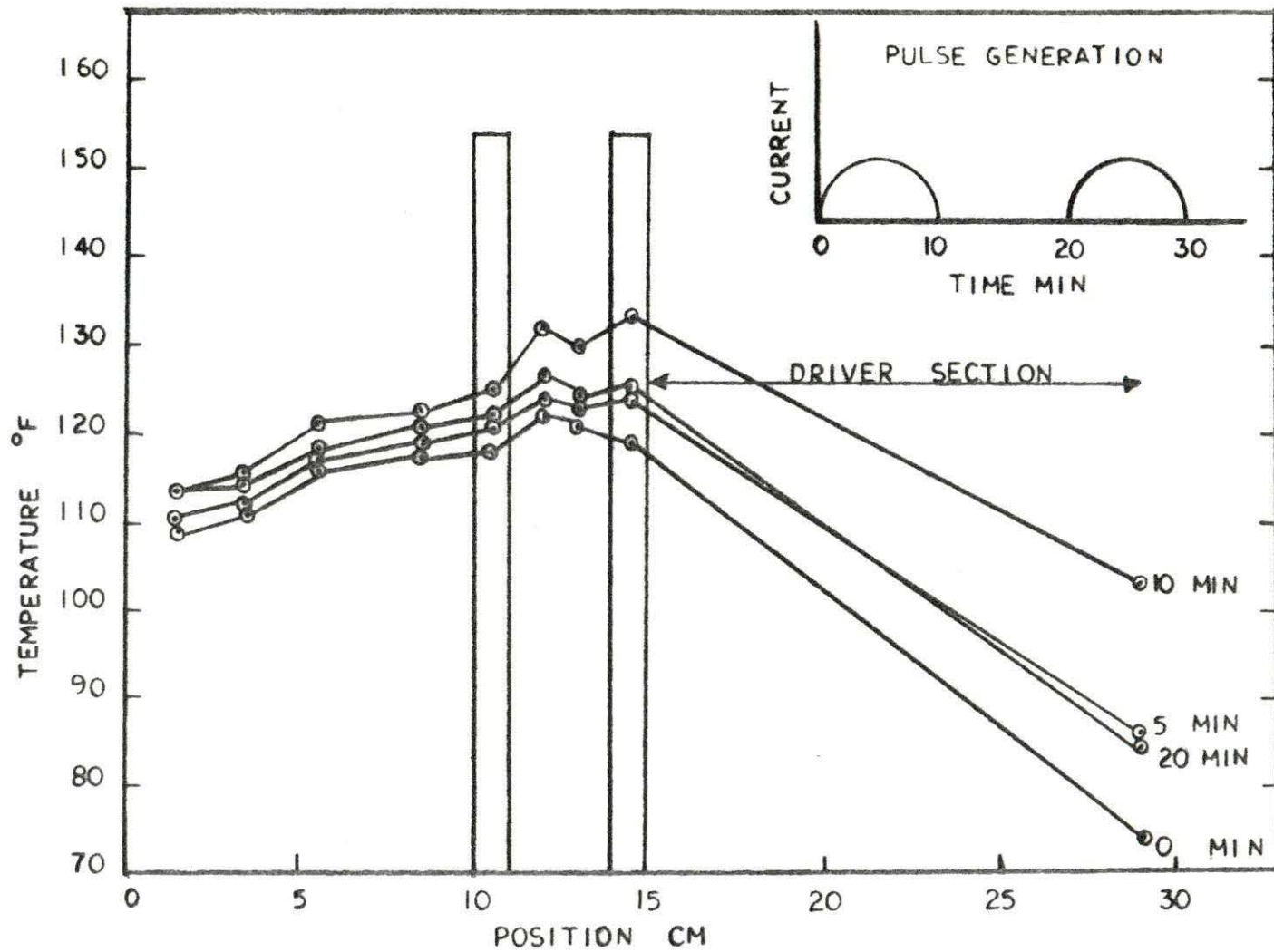


Figure 15. Variations in temperature along the rod during a heat pulse cycle without proportional control in the source region

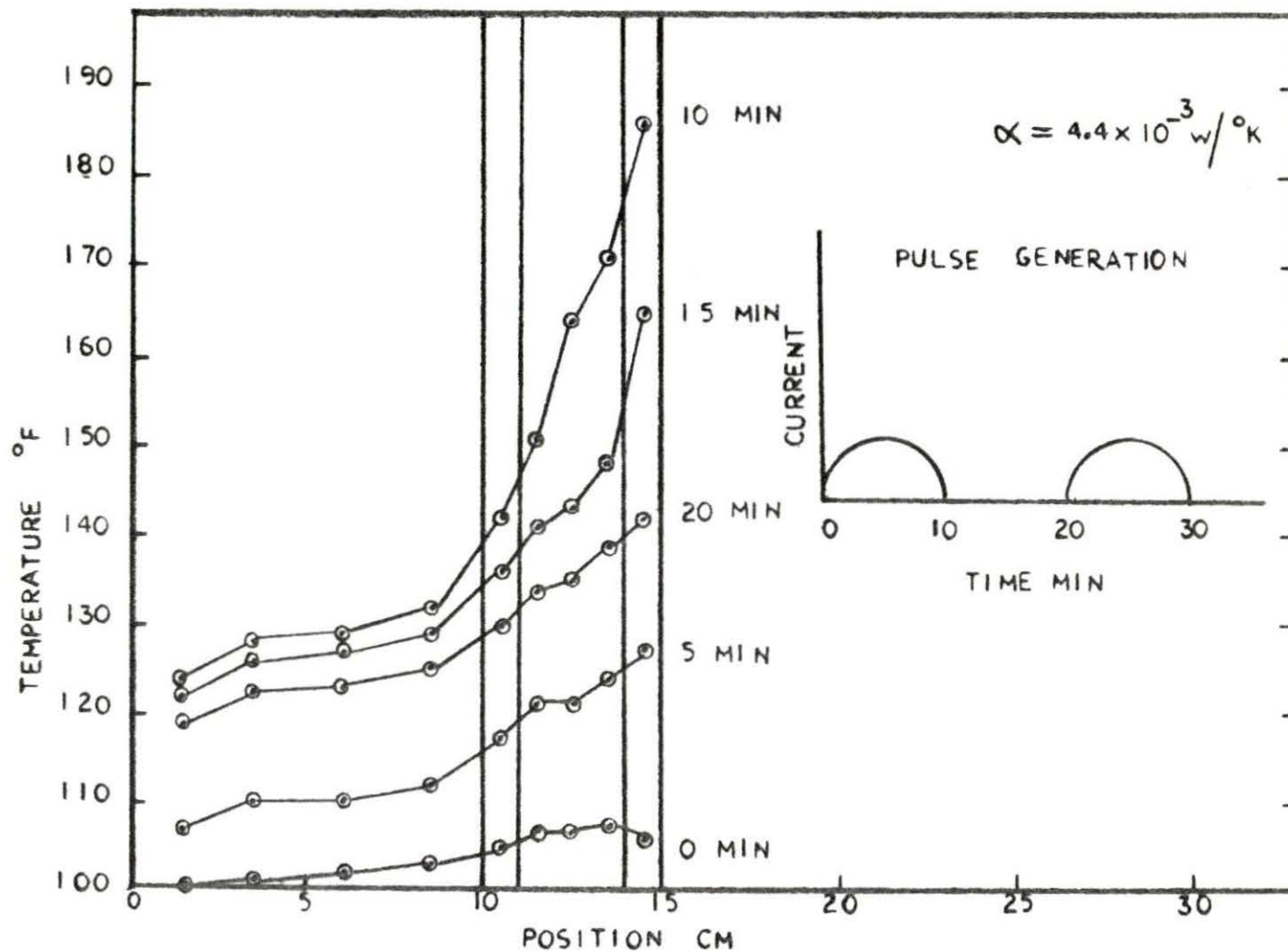


Figure 16. Temperature variations along the rod during a heat pulse cycle with proportional control in the heat source regions

intensity. With this taken into account the plots in both figures 15 and 16 exhibit the same basic shape, only varying in amplitude. The reason for using the temperature-power proportional control in the model heat source region can be justified not only by the fact that the similitude requirements demand it, but by the fact that it is more analogous to the prototype behavior. The power of a nuclear reactor can be given in terms of the product of some constant value and the neutron flux.

$$P = A \phi$$

where A includes a combination of the volume of the reactor; fission rate required to produce a specific amount of power, perhaps one watt; and the macroscopic fission cross section.

From the collection of the pertinent data it is hoped to establish relationships between the variables significant to the model study. Since the designed model was distorted rather than true, it was necessary to take data for three different models. As stated before this did not involve the construction of other models but only involved changing the distorted variables of frequency and temperature-power proportionality. Therefore data were taken for the three values of α selected. The frequencies used ranged from cycle times of five minutes up to twenty minutes. The data collected were then plotted in various ways to try to establish relationships among the significant variables and to

try to determine the effects of the distortion on power and frequency. The system response at each point was given by taking the ratios of the input peaks (recorded by a thermistor located in the driver pulse section) divided into output peaks determined at each thermistor location along the rod. Since temperatures were recorded in degrees fahrenheit, they were converted to degrees kelvin before the output-input peak ratios were taken. Since data was recorded for two cycles at each frequency, the plots of the data included the peak ratios as a result of the first pulse cycle and the peak ratios as a result of the second pulse cycle. Since plots of the system magnitude response versus frequency displays the dip corresponding to the sink frequency in the prototype, the model response was plotted versus frequency to detect the possibility of a dip corresponding to a model sink frequency. These plots were done for each thermistor location for each value of the temperature-power proportionality constant chosen. Figures 17 through 19 show these plots. Since the results for all nine positions were similar depending on the value of α used, these are only representative plots from each α group of all nine positions. In an effort to study the relationship of the response to the frequency for three α values, plots were made using both semi-log and log-log scales. Figures 20 through 25 display the semi-log and log-log plots for the

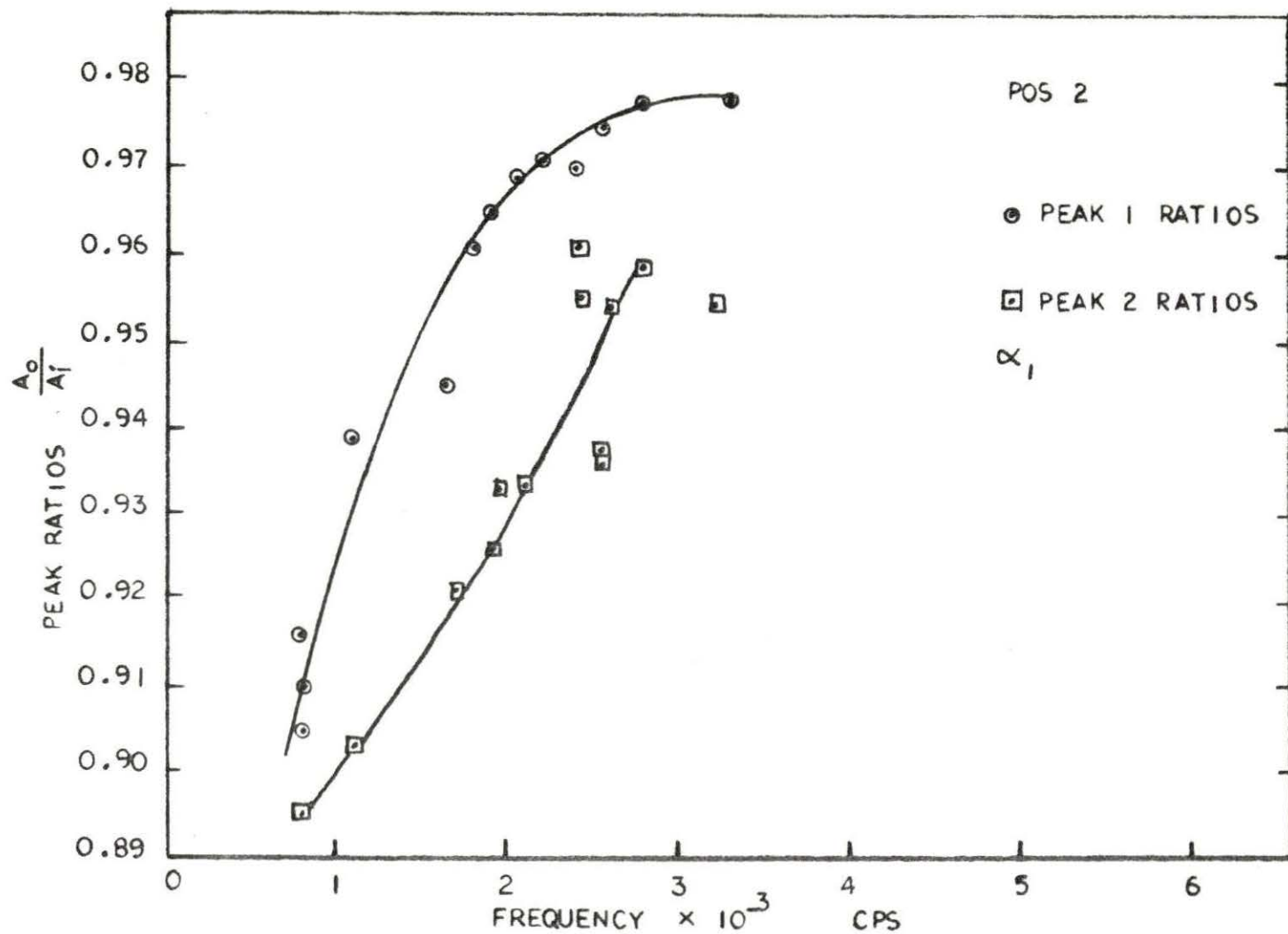


Figure 17. Magnitude of temperature response versus frequency for a thermistor location in model I

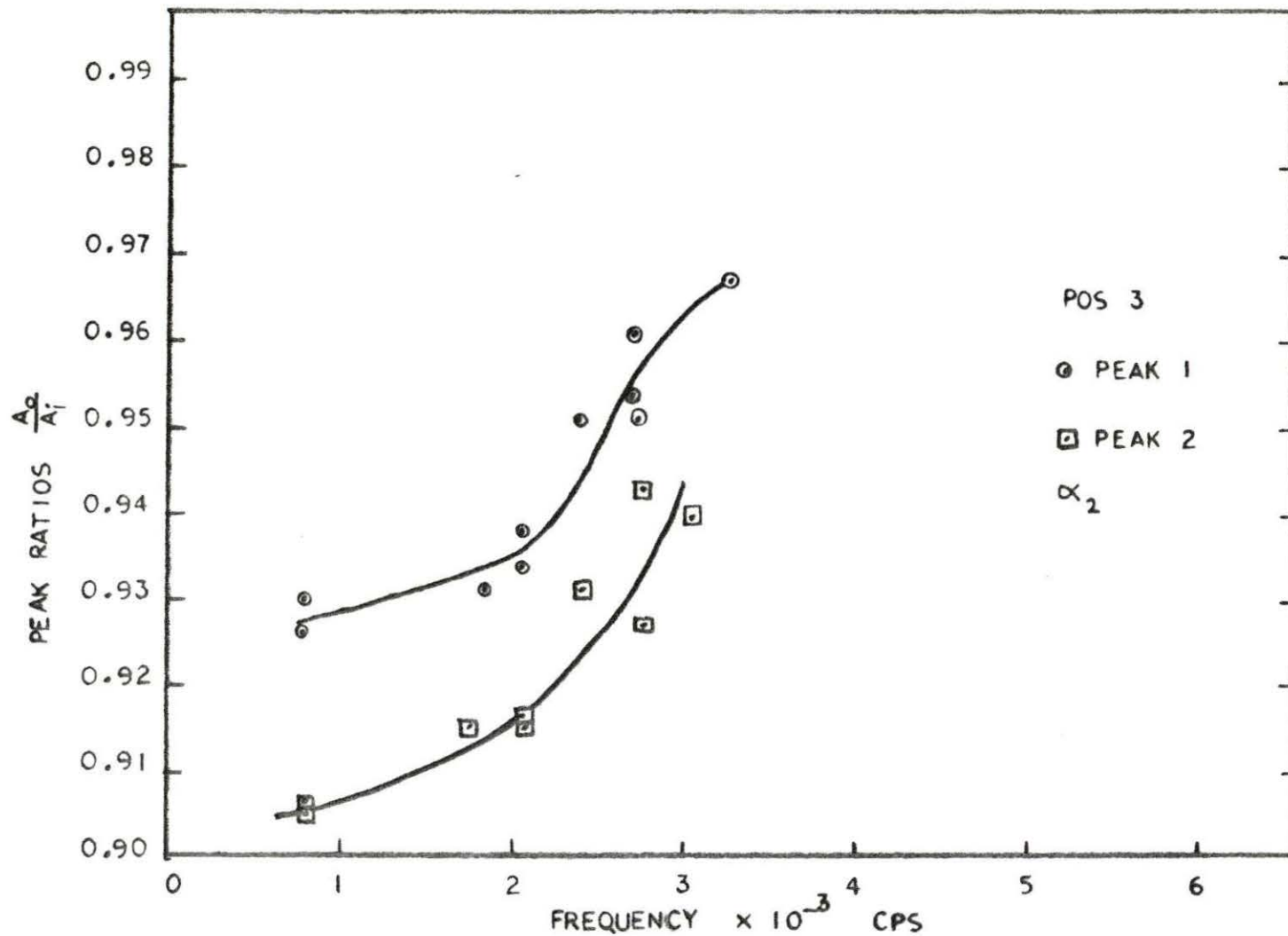


Figure 18. Magnitude of temperature response versus frequency for a thermistor location in model II

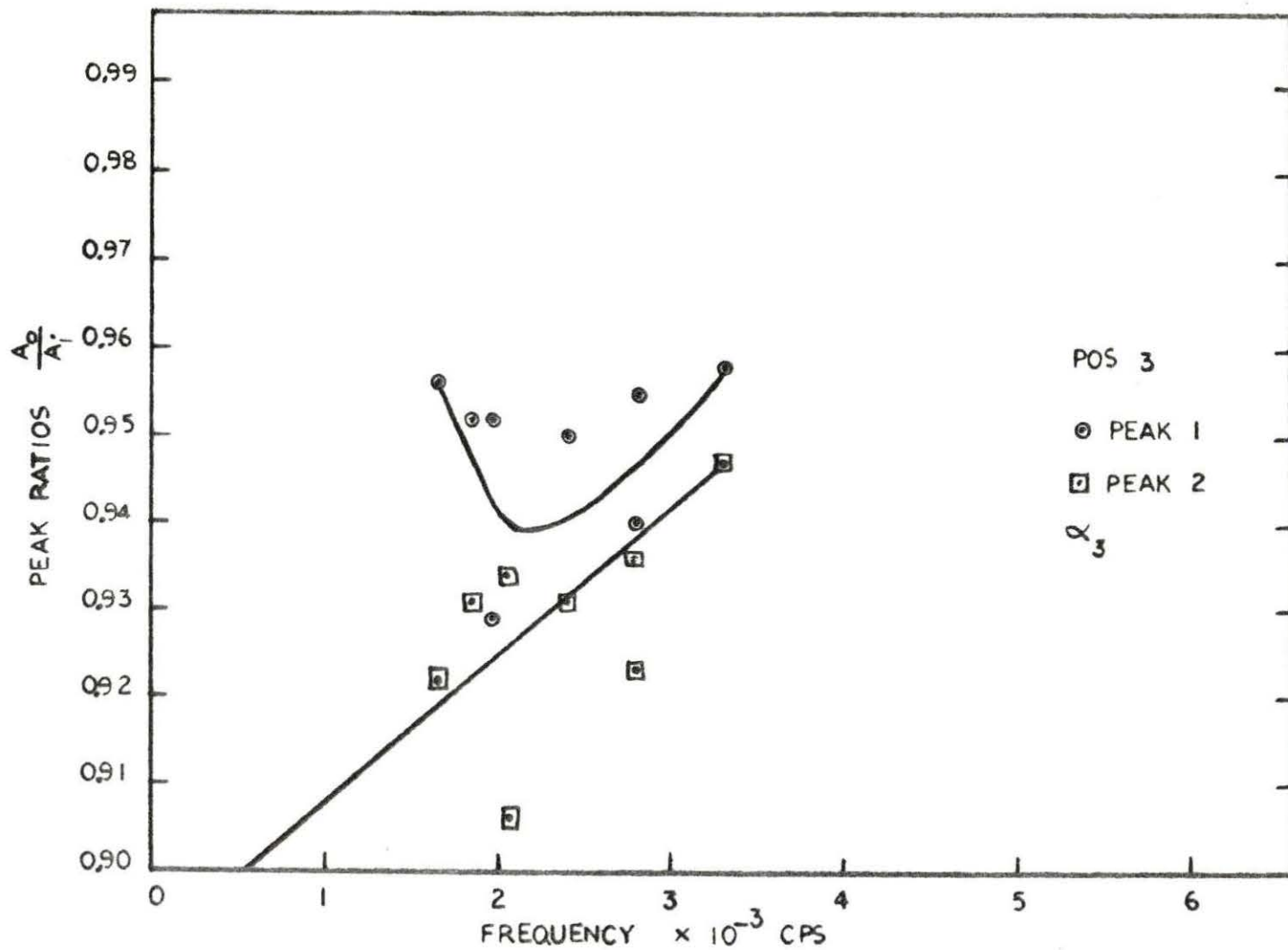


Figure 19. Magnitude of temperature response versus frequency for a thermistor location in model III

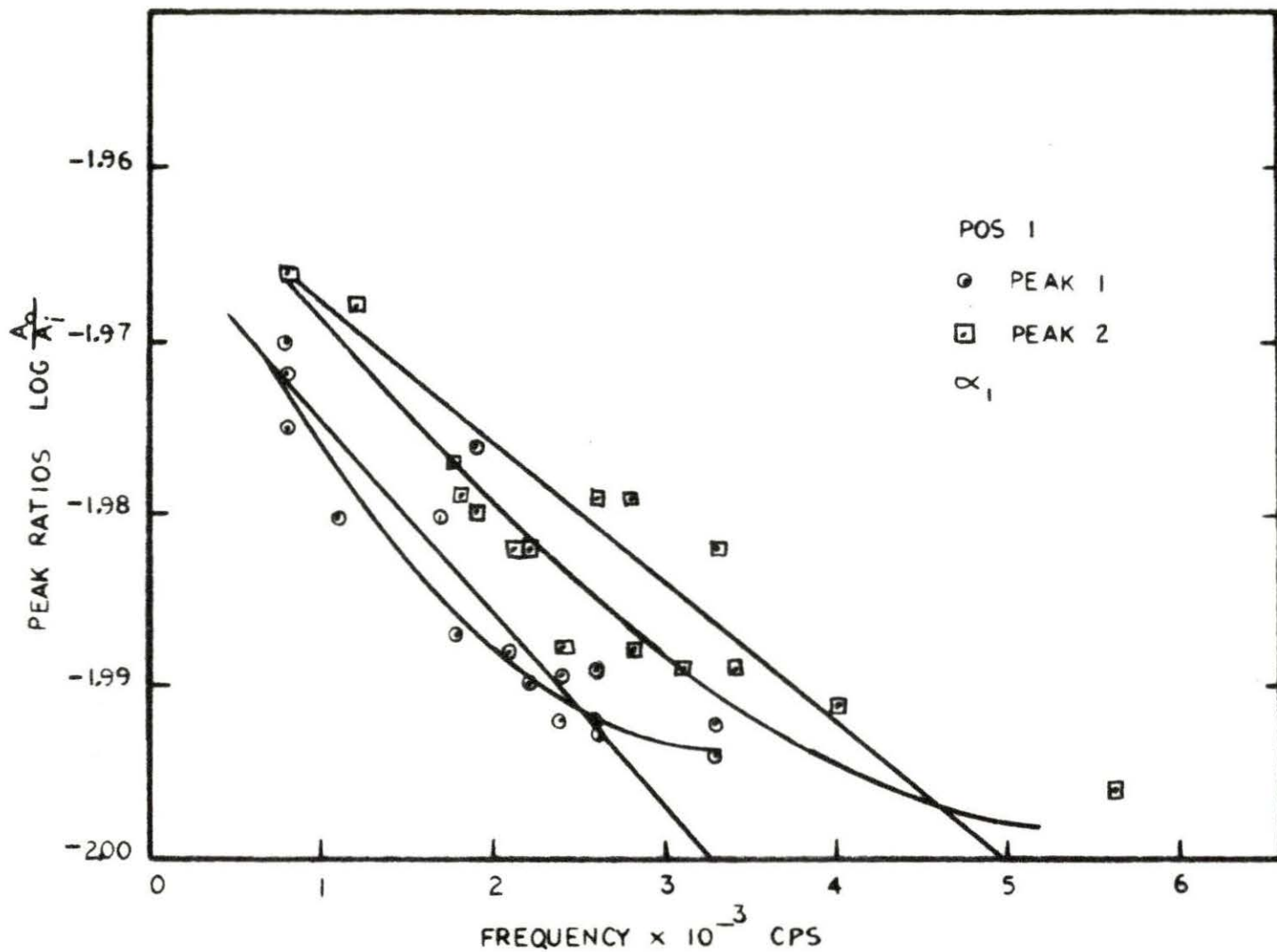


Figure 20. Magnitude of temperature response versus frequency for a thermistor location in model I

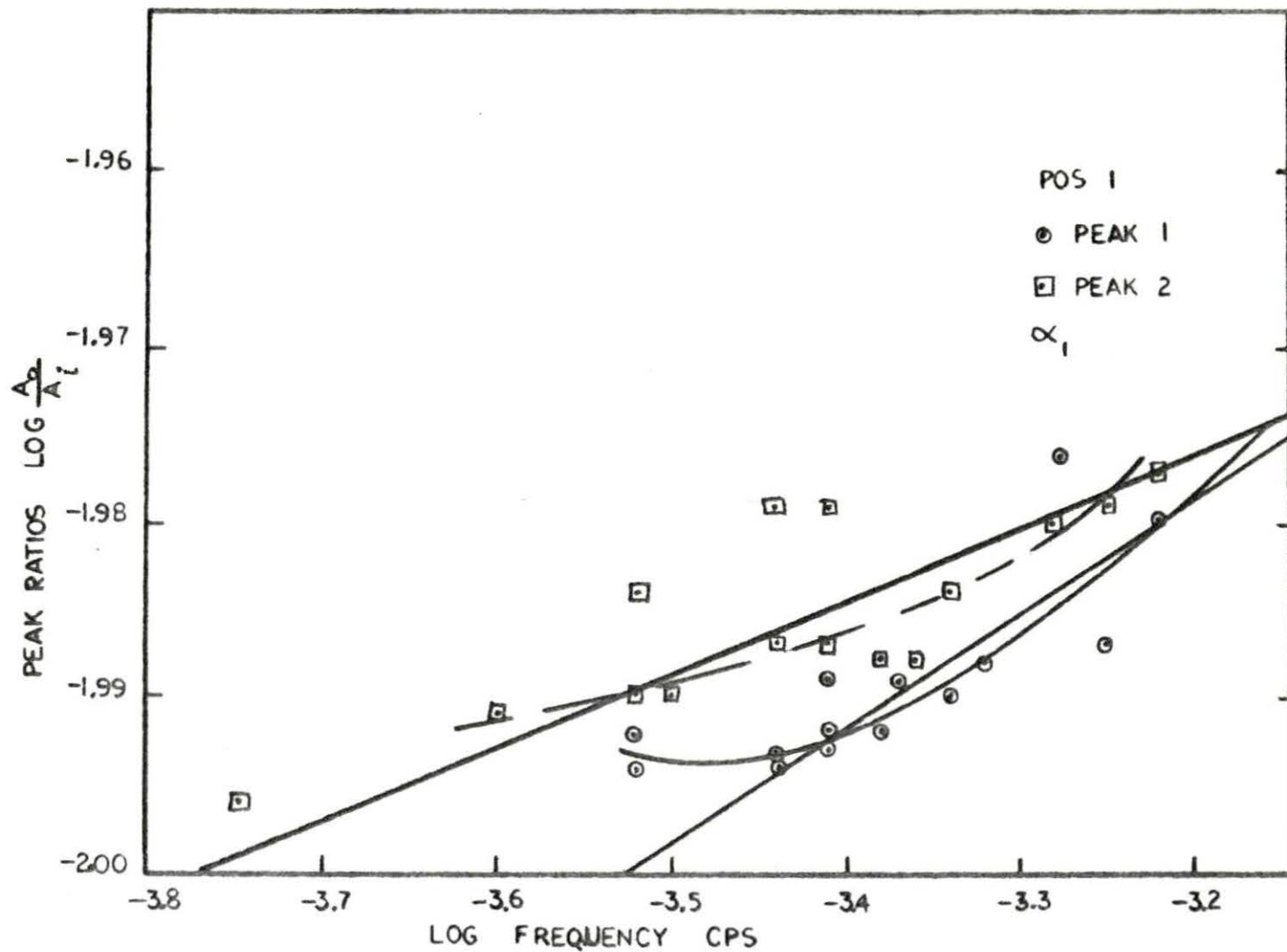


Figure 21. Magnitude of temperature response versus frequency for a Thermistor location in model I

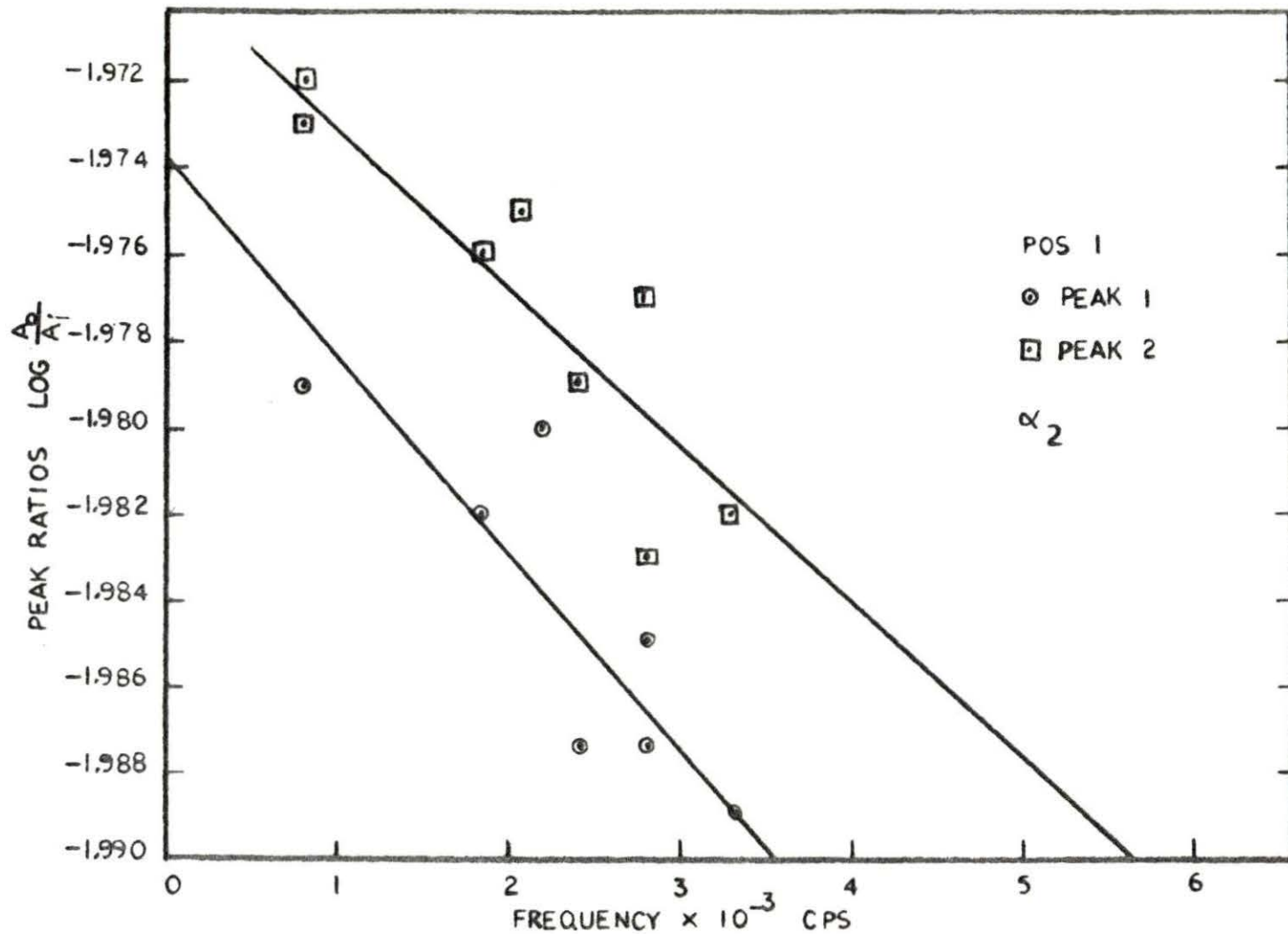


Figure 22. Magnitude of temperature response versus frequency for a thermistor location in model II

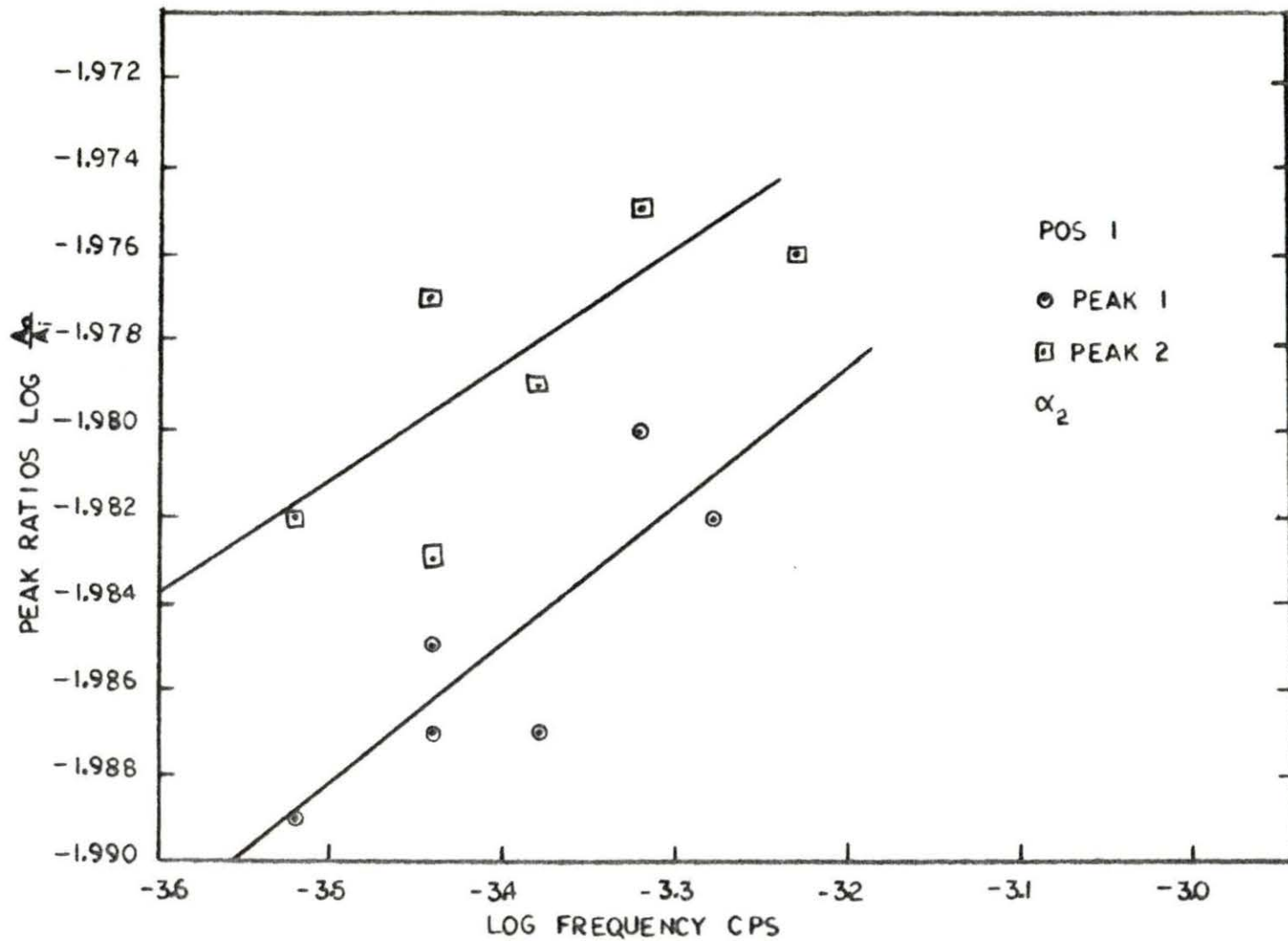


Figure 23. Magnitude of temperature response versus frequency for a thermistor location in model II

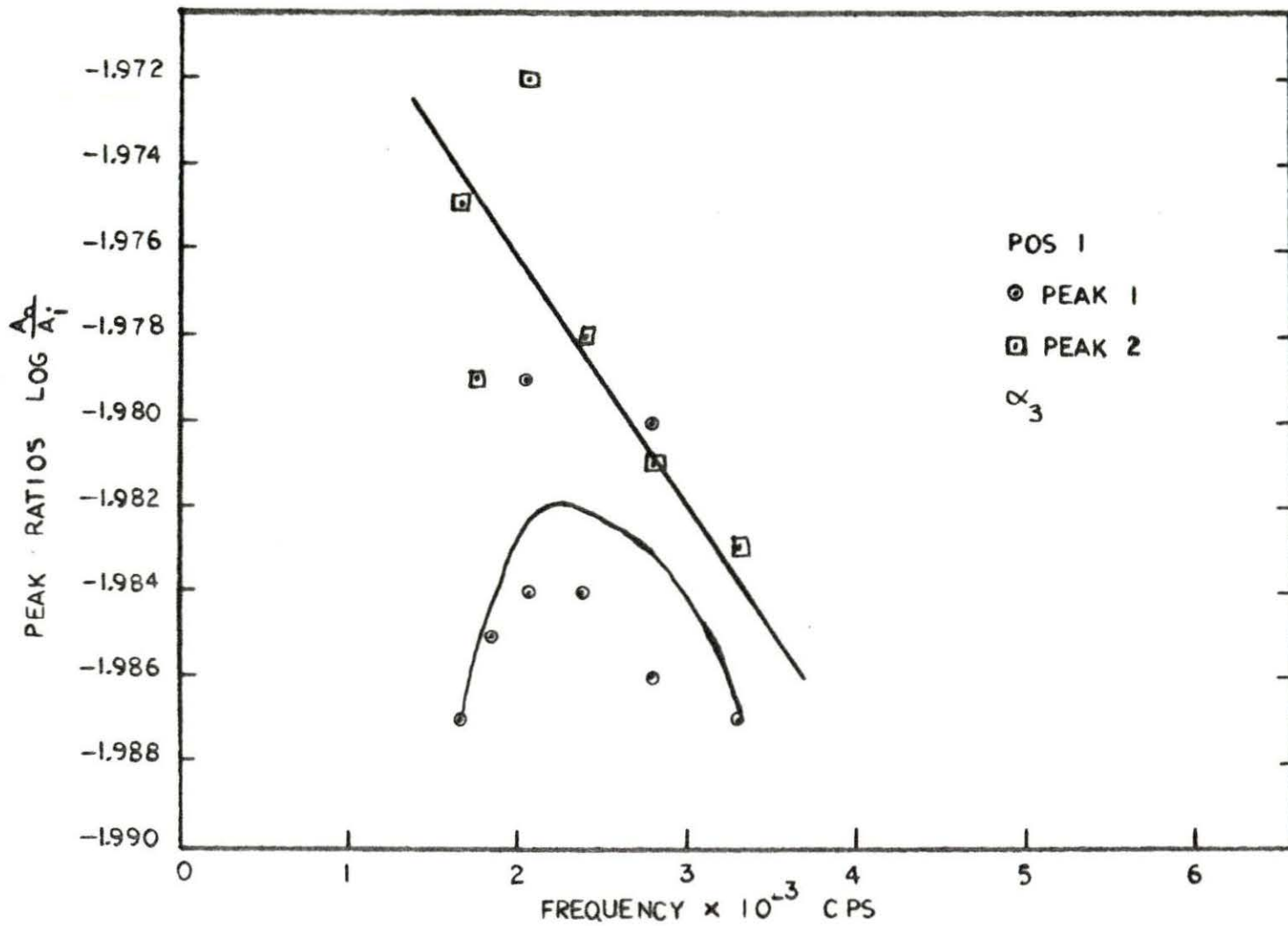


Figure 24. Magnitude of temperature response versus frequency for a thermistor location in model III

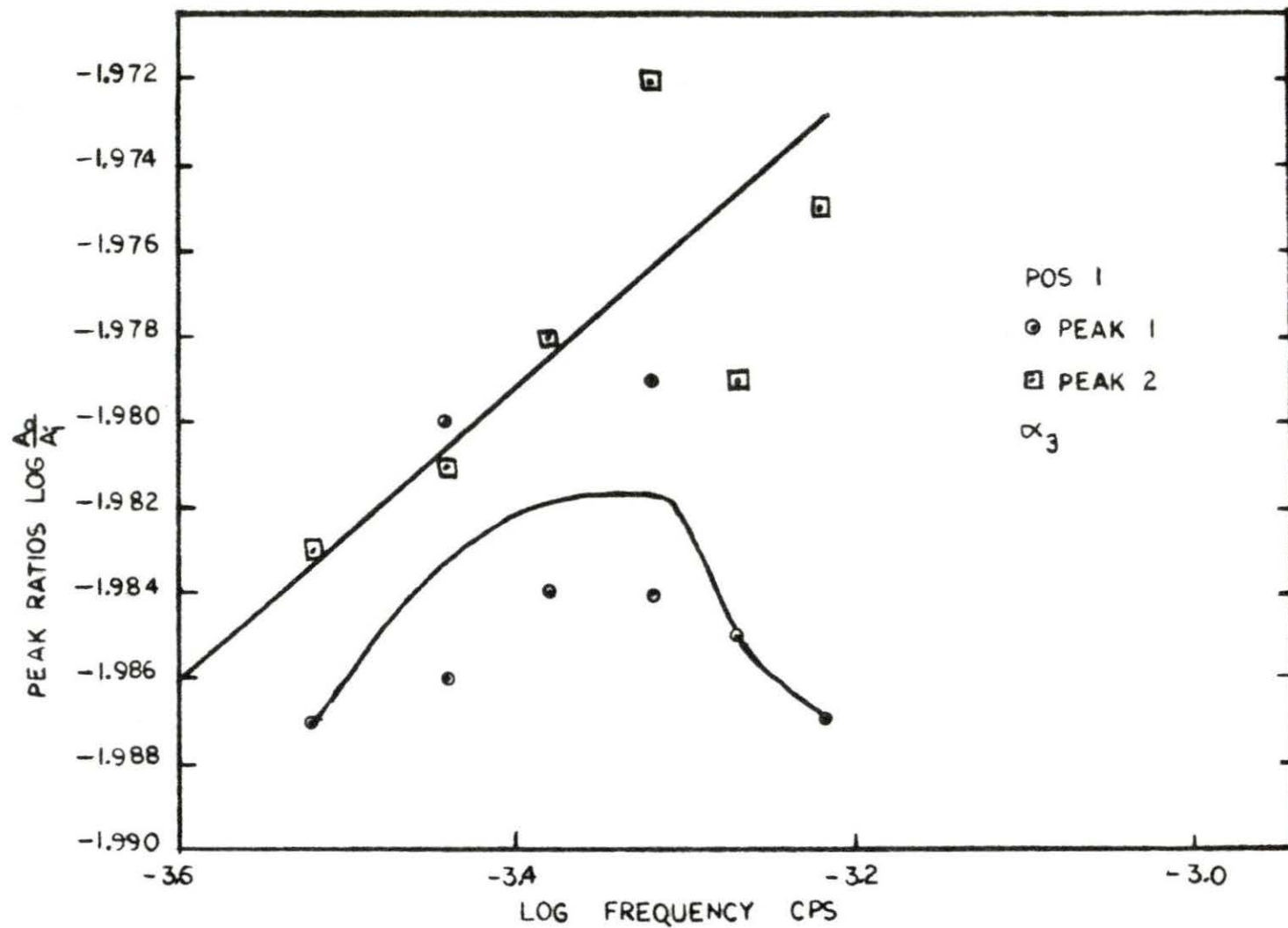


Figure 25. Magnitude of temperature response versus frequency for a thermistor location in model III

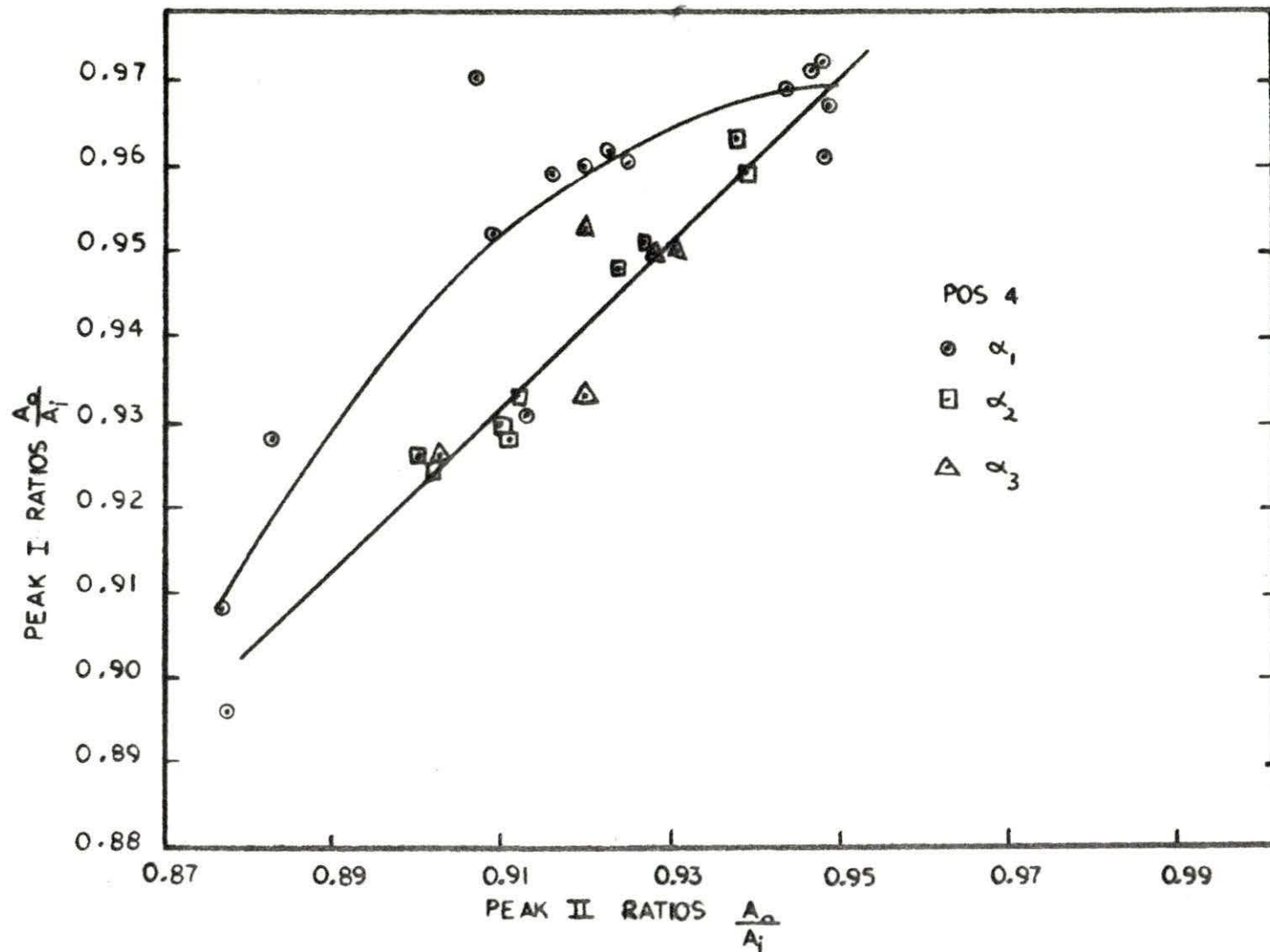


Figure 26. The relationship between peak I and peak II ratios at a thermistor location for all three models

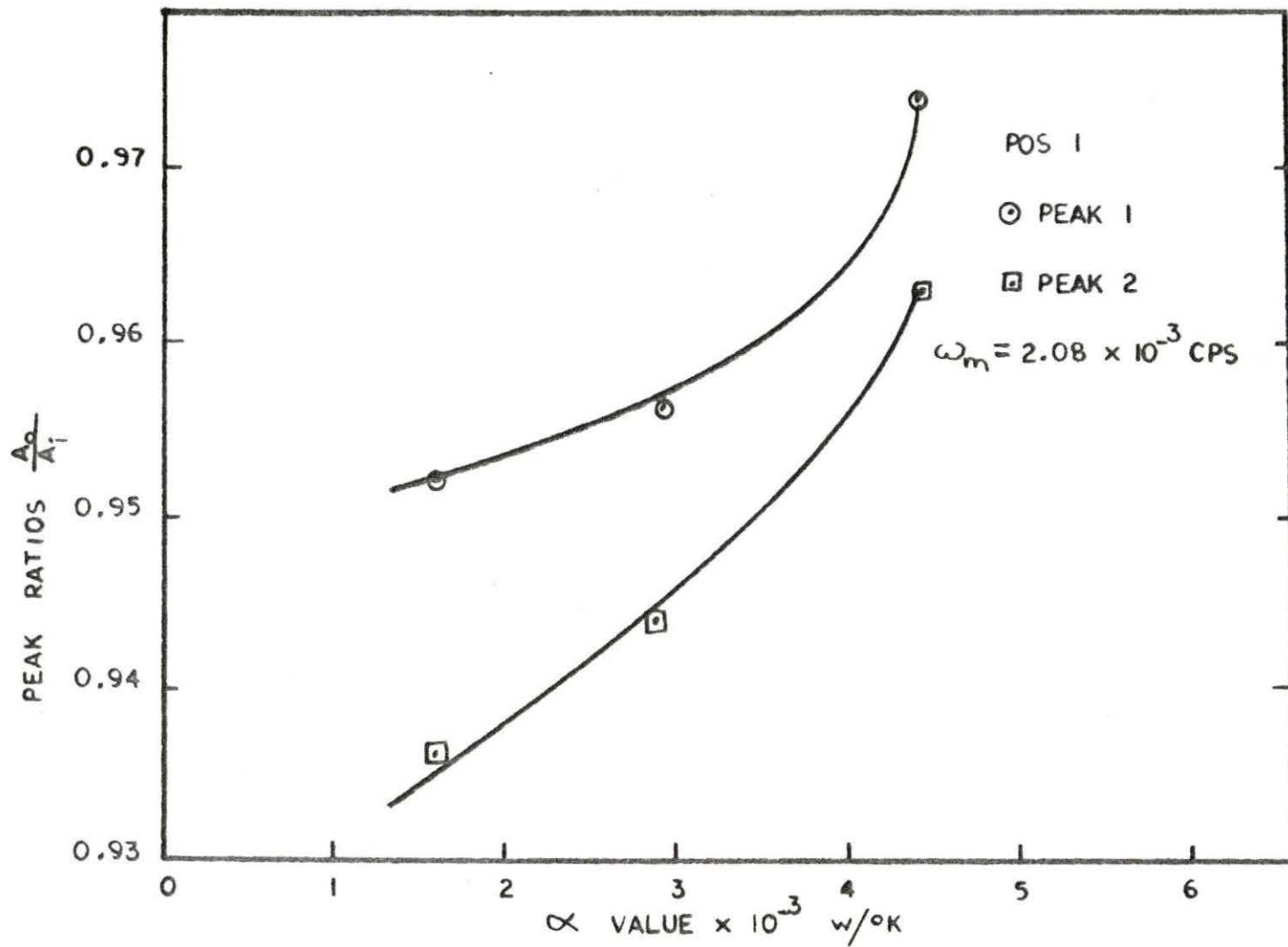


Figure 27. Magnitude of temperature response versus values for a frequency and a thermistor location

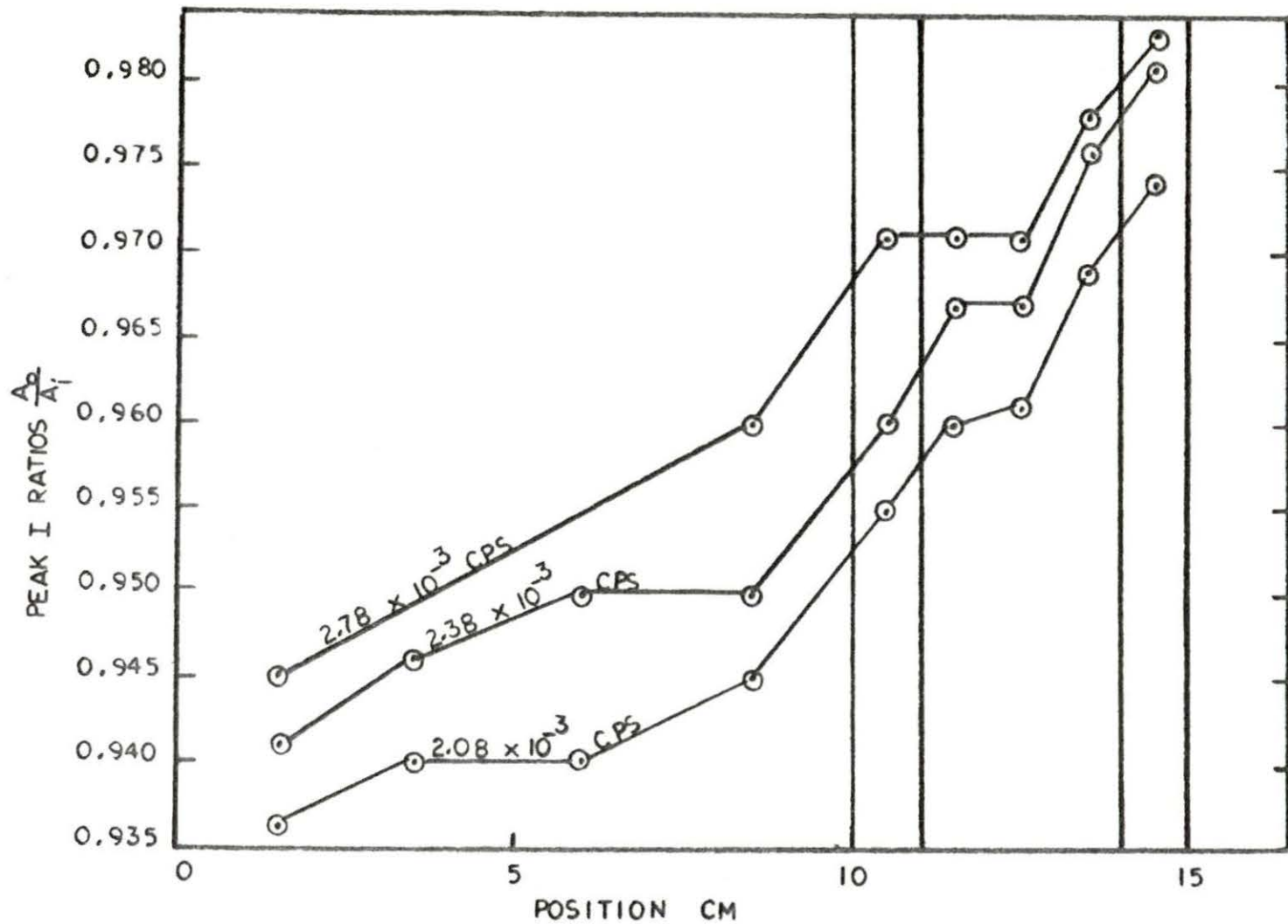


Figure 28. Peak I ratios versus model I thermistor locations for three frequency values

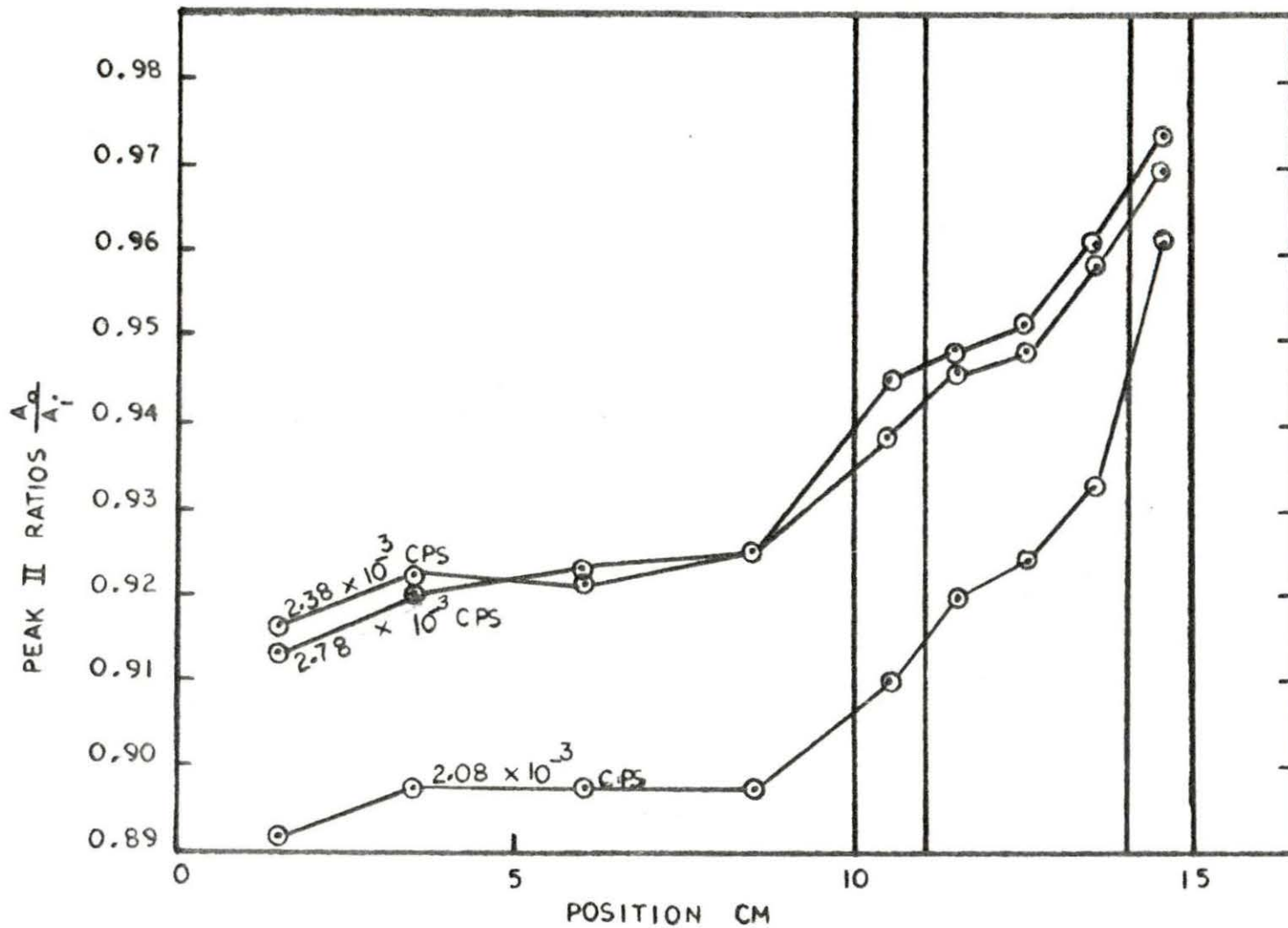


Figure 29. Peak II ratios versus model I thermistor locations for three frequency values

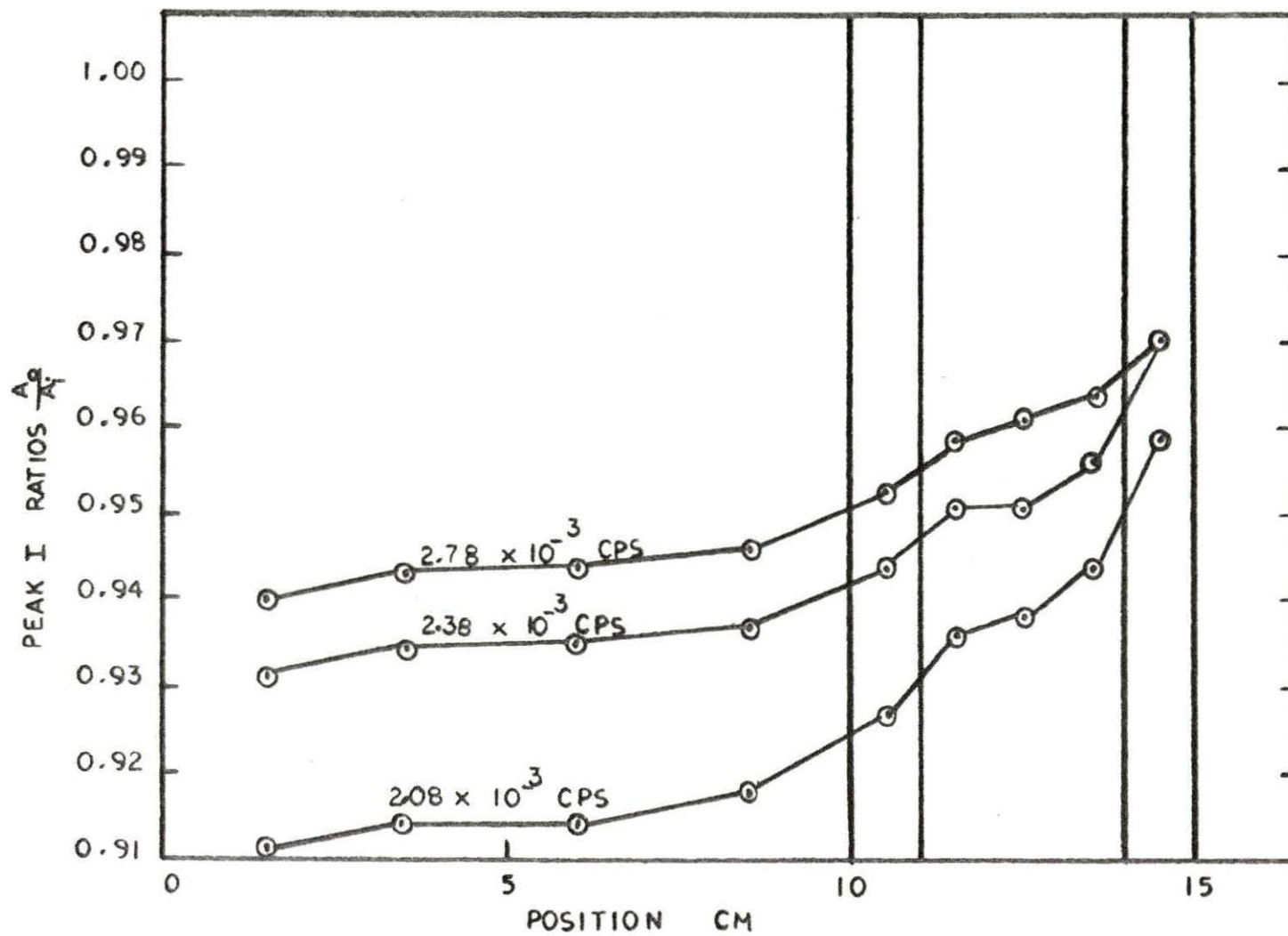


Figure 30. Peak I ratios versus model II thermistor locations for three frequency values

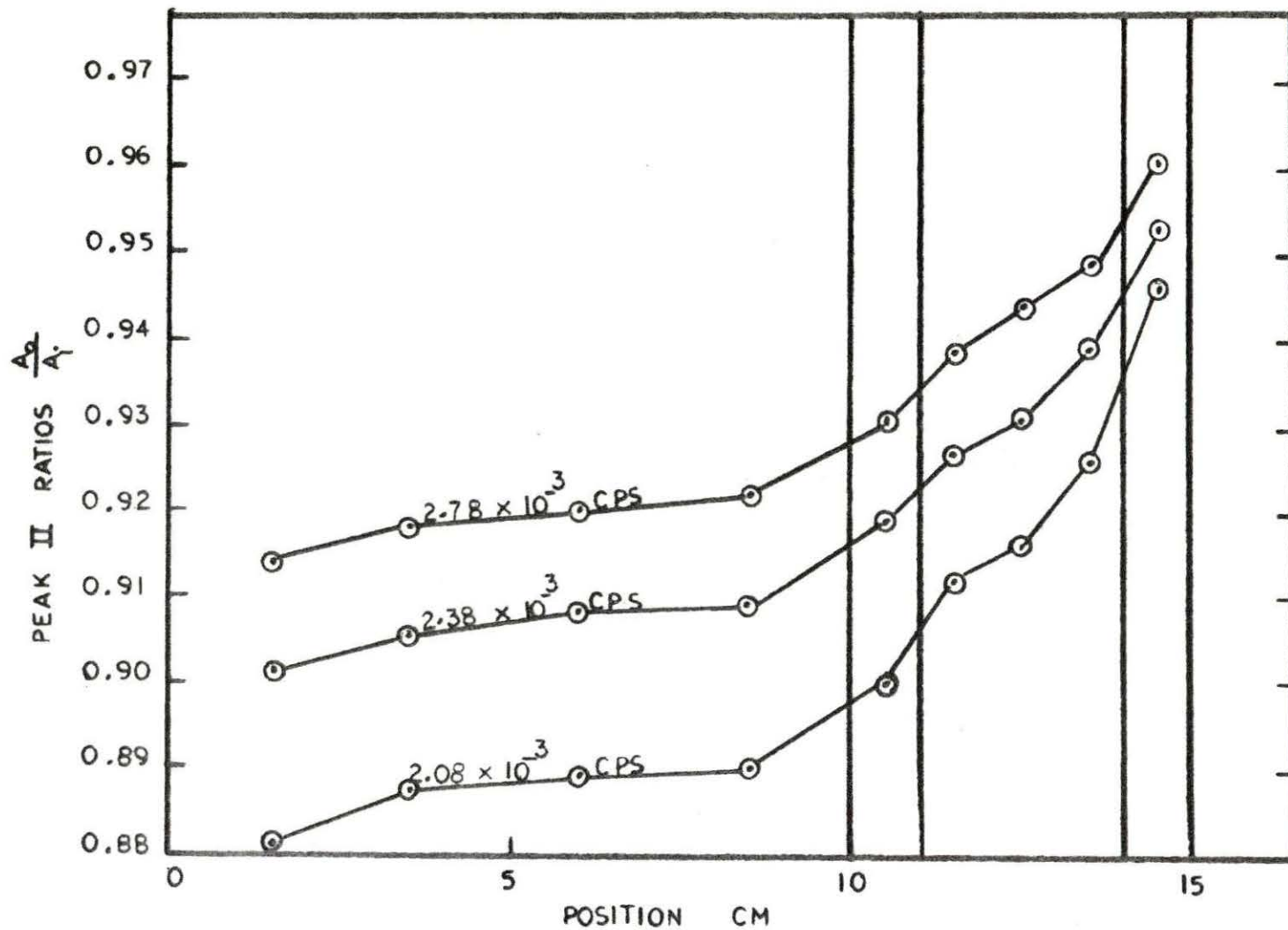


Figure 31. Peak II ratios versus model II thermistor locations for three frequency values

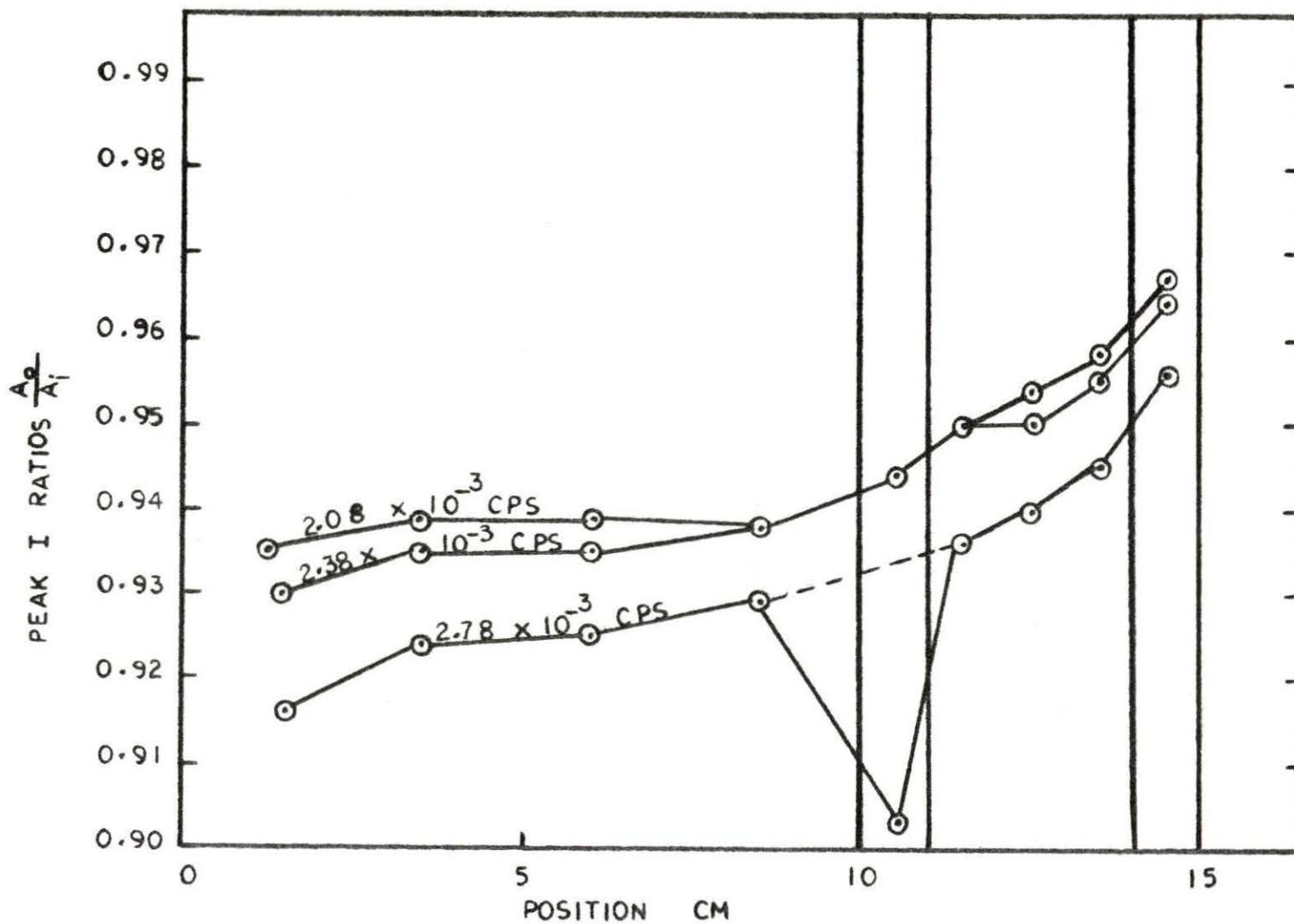


Figure 32. Peak I ratios versus model III thermistor locations for three frequency values

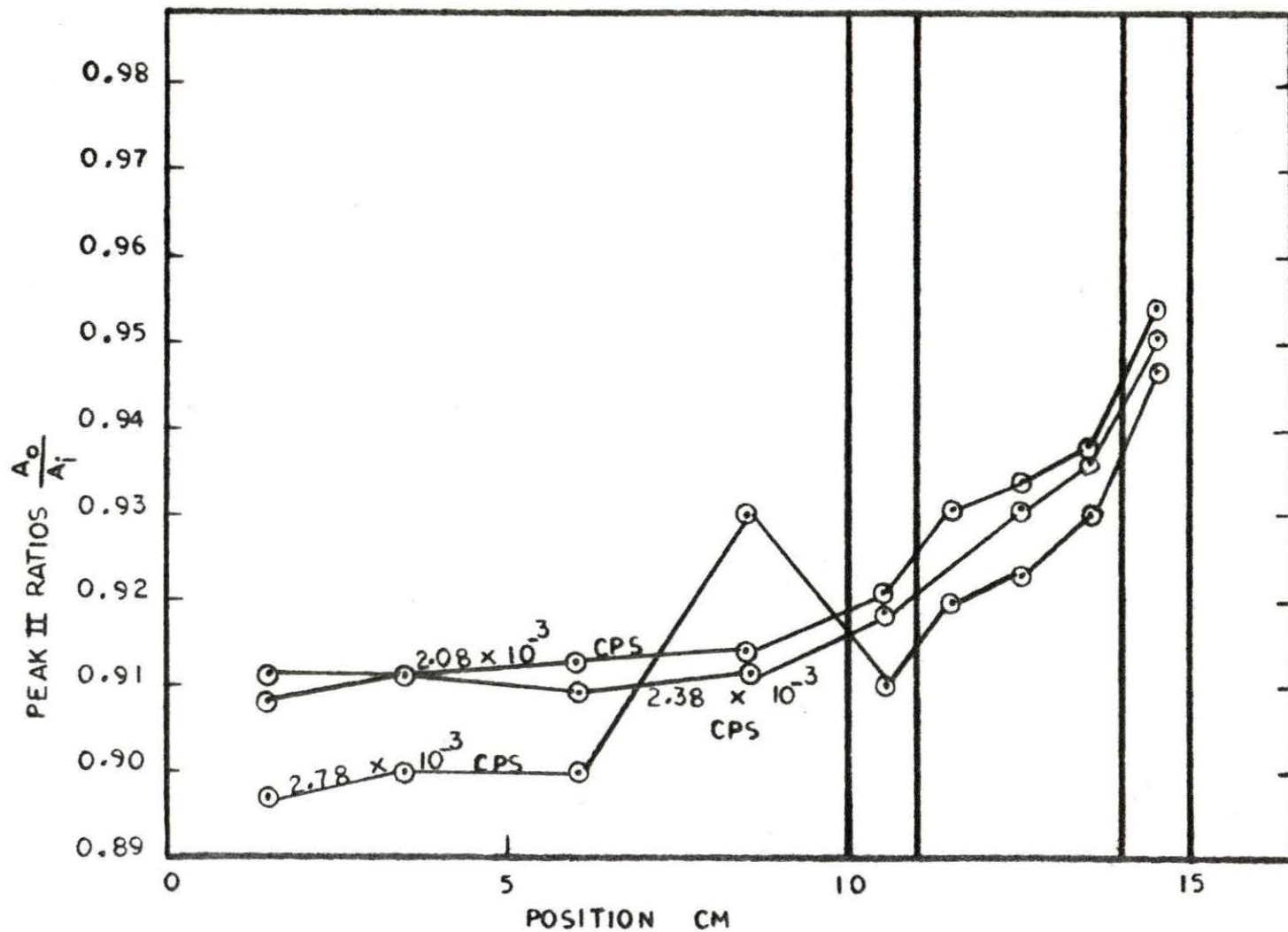


Figure 33. Peak II ratios versus model III thermistor locations for three frequency values

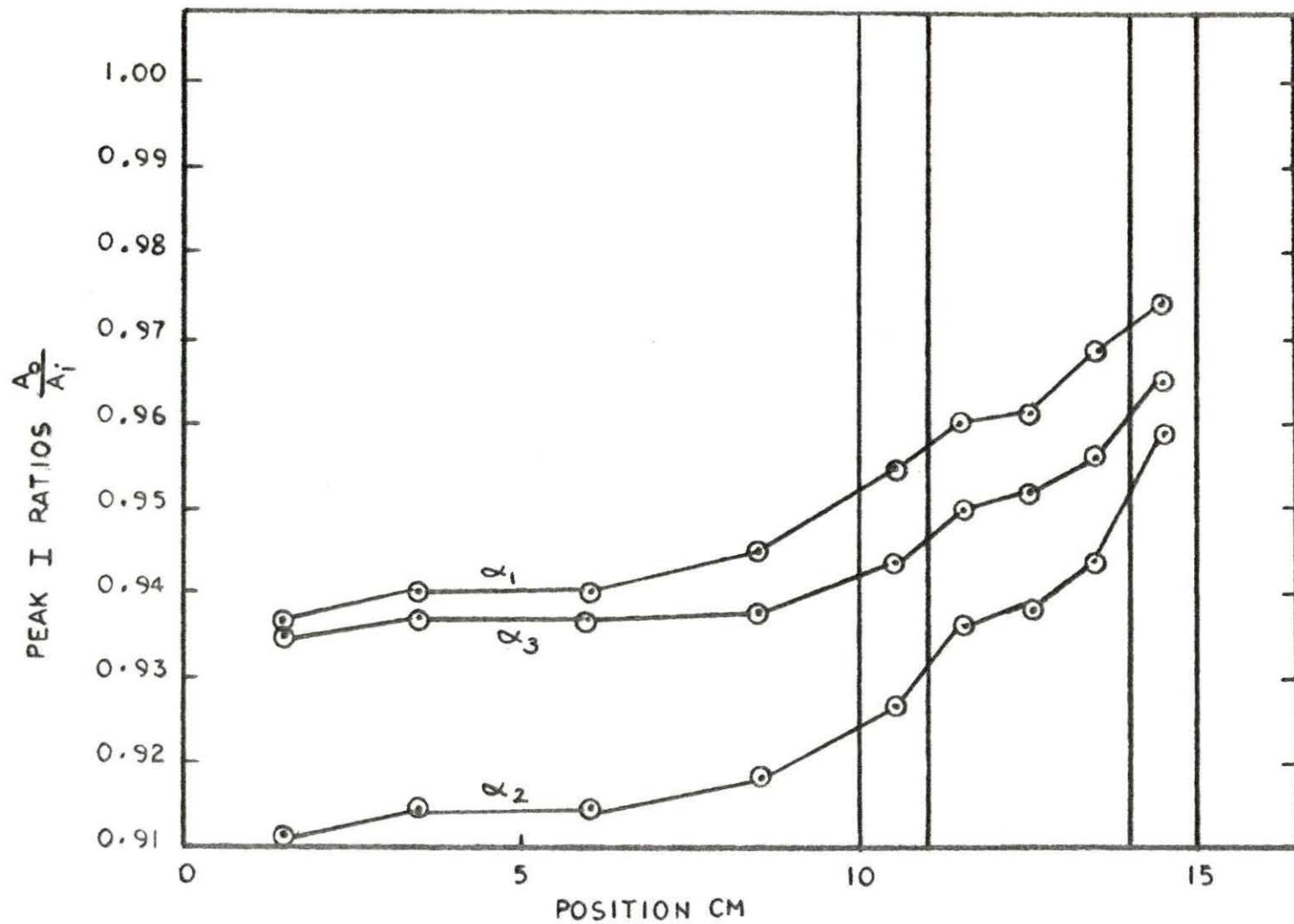


Figure 34. Peak I ratios versus thermistor locations in the three models for a frequency run

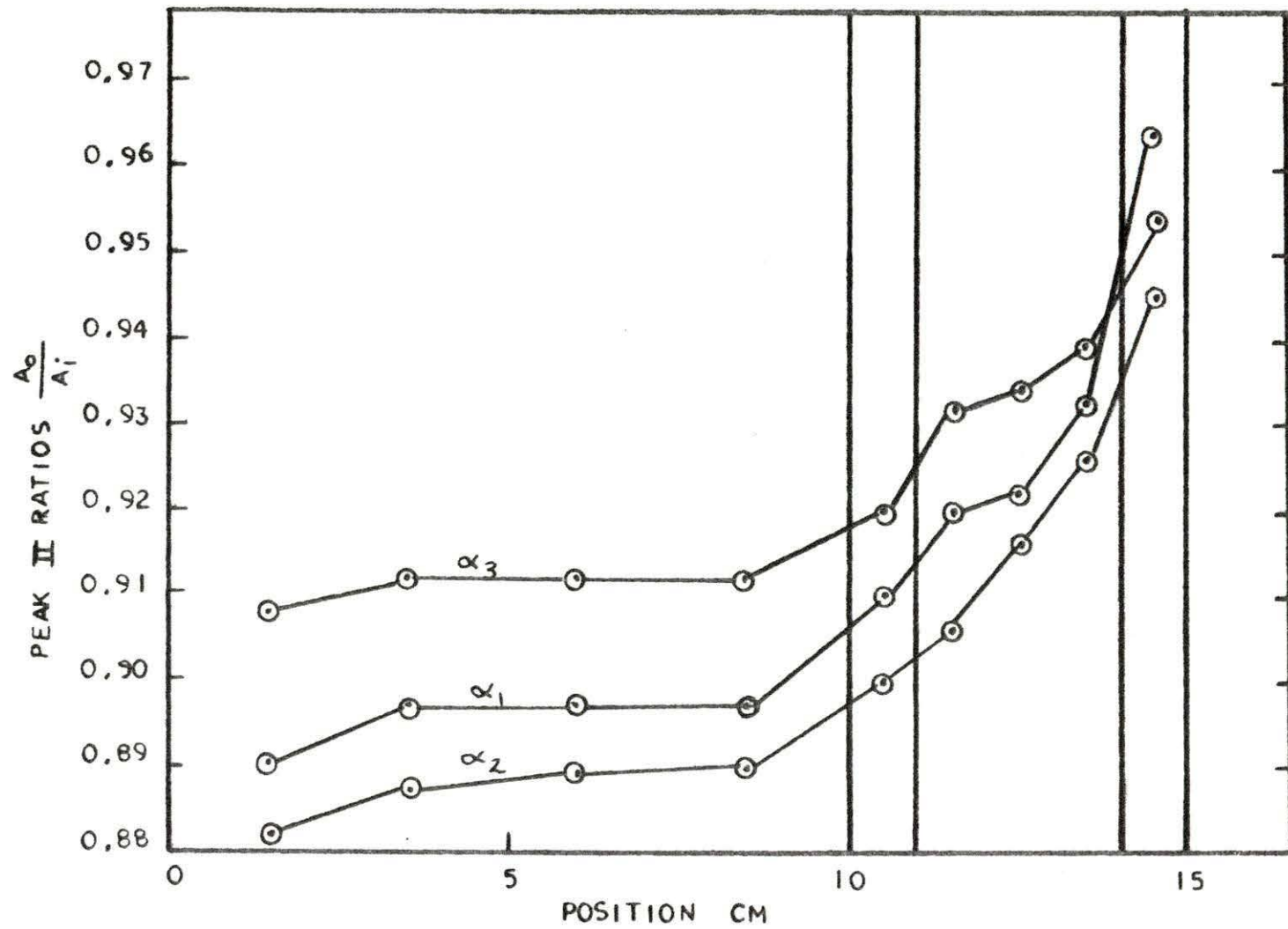


Figure 35. Peak II ratios versus thermistor locations in the three models for a frequency run

response versus the frequency at a given α value for a representative thermistor location.

Also of interest is the relationship between the peak I ratio and the peak II ratio at each thermistor location on the model. Figure 26 shows the relationship of peak I to peak II values for all three α values at a representative thermistor location. The plots for the other eight positions display the same characteristics.

To aid further in determining the effect of the distortion on the model other plots were made as follows. Since the peak ratios were plotted versus frequency for three constant α values, graphs were also made of peak ratios versus α values for three different values of frequency. This time with constant frequency values it is desirable to establish a relationship between the ratios and temperature-power proportionality constant. Figure 27 is a representative plot of the relationship between the response and the proportionality constant. It is a representative plot because the same graph for other frequency values displays the same behavior. Finally to observe the effect of value and frequency (hence the distortion on the model), plots were made of the system response, or peak ratio versus position for values of constant frequency and constant values. Figures 28 through 33 show plots of peak ratios versus position for three frequency values, each at a specific

α value. Figures 34 and 35 show representative peak I and II ratios versus position for three values of α at a specific frequency value.

DISCUSSION OF RESULTS
AND ERROR CONSIDERATIONS

Figures 17 through 19 indicate that for each value of alpha considered, the peak ratio frequency curves have the same form for all nine thermistor locations. So the response to the heat pulse at one point in the model indicates its form at the other eight positions for a given alpha value. Graph 17 shows that for model I with $\alpha = 4.4 \times 10^{-3}$ w/°k both peak ratios show the same form, although peak I ratio frequency plot is higher than the same plot of peak II ratios. This occurs because in the second cycle the peaks attained at the various positions are almost the same height attained during the first heat pulse cycle. However, the heat input perturbation pulse attains a far larger peak in the second cycle than in the first. Therefore the ratios of the peak outputs to the input peak for cycles I and II show peak II ratios at a lower value than peak I ratios. Reference to figure 13 shows a comparison of output peaks for each cycle and input peaks for each cycle. The larger increase in the input pulse height during the second cycle can be explained by the fact that the driver section is better insulated than the rest of the rod and hence the second pulse always starts on an additional thermal level and attains a higher peak. The heat in the driver section isn't lost as readily to the surrounding air as at the other thermistor locations along the rod. This plot for model I in-

indicates no dip corresponding to a model sink frequency. The graph 18 refers to model II with an α value of 2.85×10^{-3} w/°k. Model II was operated in a lower power range as indicated by the lower α value. However, the two peak ratios have the same form, but the peak I ratio is higher than the peak II ratios. The form of these curves is very similar to the forms seen in model I plots, excluding the slight distortions in the initial parts of the curve. Model III corresponding to an α value of 1.59×10^{-3} w/°k was operated in the smallest power range. The response here appears to be less favorable in regards to both models I and II. Again the peak II ratios occur at lower values than the peak I ratios. The peak I ratio however is totally different in form than the corresponding curves in the other two models. The peak II ratio points appear to be largely scatter points. The line of best fit for these points a slope similar to the corresponding curves in the other two models. It can be assumed that the peak I ratios of model III show no real dip or sink frequency. This is based on the fact that the other data trial points at the same frequencies do not duplicate a true dip behavior. They do indicate what could be considered a small ripple in the total picture of all points beginning from the origin. In consideration of the plots of the other models and the behavior of the peak II ratios of model III, the peak I ratio plot is to be viewed with larger error than the other data

points. Just as in the case of model I and II, model III shows no sink frequency. From these plots for the various alphas at a particular position, the ordinates in reality vary very little when considered in light of the origin or the zero point on the y axis. In view of the limited range of data points shown on the graph, the plot can be thought of as small variations in an overall curve beginning at the origin. Figures 20 to 25 show that within the limits of the experimental data, in other words the portion of the total curve beginning at the origin, the peak ratios can approximately be shown as a line when plotted on logarithmic scales versus frequency, depending on the accuracy of the lines drawn. Model I still shows slight curvature in figures 20 and 21, but can also be roughly approximated by a straight line. Model II can also be roughly approximated by a straight line. Model II can also be roughly approximated by a straight line as shown in figures 22 and 23. Model III shows that the peak I ratio frequency curve retains its unusual shape no matter how plotted; while the peak II ratios plot with a rough straight line approximation. These plots on logarithmic scales for all the models show fair agreement in all cases, except the peak I ratio plots for model III.

Graph 26 relates the peak I ratio to the peak II ratio at a position for all three models. As might be expected the curves are fairly linear. Models II and III show the

same linear relationship between the peak I ratio from the first cycle and the peak II ratio from the second heat pulse cycle. The effect of the temperature-power proportionality constant of the three different models is not important to the relationship between the peaks. The peak ratios from the two cycles for the model I position shows slight curvature and significant deviation from the linear plot of the values for models II and III. Thus the peak II values in model I increase at a non-linear rate compared to the peak I values. A linear relationship might be expected among peak I and II values. During the heating part of the heat pulse the rod heats up to a peak value, then during the non-heat part of the cycle the rod cools down to a lower value, but not back to the original initial value. By the time the second heating part of the next cycle is started the temperature still hasn't dropped to the original value. This means that the second pulse peaks a little higher as a result of starting from a higher temperature level. For different frequencies the cooling period varies according to the length of the non-heat part of the cycle. At the same time power is generated in the cores proportional to the temperature as it may rise or fall. For models II and III this core power level is smaller than for model I. The effect of the proportional control in the cores is less pronounced for the two smaller alpha values of models II and

III. Model I has a greater effect of the power proportional control and influences more the level on which the second peak builds. Figure 27 shows that at each frequency value the peak ratios tend to rise in a fairly linear fashion with each increasing alpha value.

The plotted results have shown that the system response as a ratio of output to input peaks for both cycles I and II, increases with increasing frequency; within the limits of the data range of points this peak ratio increase shows some form of exponential rise with increasing frequency for the logarithmic scale straight line approximations. For each frequency value the peak ratio of response increases fairly linearly for model values of alpha in cases II and III, but model I exhibits slight variations in a few frequency runs. Using this information plots were made to determine the effect of these conditions on the temperature peak ratio response as a function of the thermistor locations along the rod. Figures 28 to 33 show a general trend of the space plot of the peak ratios to increase with increasing frequency. This is especially true for models I and II, particularly for peak I ratios. The peak II ratios also exhibit this behavior, however in model I, the peak II ratios almost coincide and overlap, for the longer frequencies or shorter cycle times. The same plots shown for model III indicate that the exact reverse is true; for increasing frequencies the space peak ratios curve decreases in the

cases of both the peak ratio values. This behavior further supports that error is most likely shown in the behavior of model III. Figures 34 and 35 give further information by showing the space peak ratio curve as a function of the alpha value for a specified frequency value. These curves show that at a particular frequency value the peak ratio response increases with increasing alpha value, for models I and II, but not in the case of model III data. In view of figures 28 to 31 and figures 32 and 34, the unusual dip in one case and peak in the other case indicates probable error at these points for model III.

Thus it is shown that the relationships between the peak ratios and the alpha values and the frequencies seem to be consistent for the same ratios as a function of time and space for all the models studied, except in one instance for model III. The major discrepancy shown here is the reverse behavior of the peak ratio space curve for various frequencies at a given alpha value. It is felt that the data from model III is misleading as a result of the lack of satisfying one of the similitude requirements - that of proportional core control. The reason for this goes back to the fact that at this low value of alpha in model III the temperature changes were so small until the temperature-power proportional control of the two cores was almost non-existent within the range of the equipment available. So basically these data points are not valid as in the case

of the other data points where in the other models the changes in the temperatures in the two cores was large enough to warrant the manual porportional control. Earlier it was stated that this effect coupled with the various frequencies help to determine the peak levels for a particular cycle. So if the proportional control in the cores was neglected then the rod just heated up more during a slower heat pulse frequency than for a faster one. Conversely, the other models do exhibit the effect of the proportional control, since their space peak ratio profiles increase with increasing frequencies or faster cycle times. This is again explained by the fact that the input peaks are much larger than the output peaks for slower cycle times, hence the output to input ratios of the peaks is less and less for longer cycle times at a given alpha value.

Experimental errors may be classified in these groups: errors in the equipment, errors in collecting data, errors in calculations as a result of determining true peak values for certain thermistor locations at certain frequencies. The errors in the instruments can be seen from the per cent accuracies given in the list of equipment for each instrument used. The transformer supplying core I with current displayed a continuous tendency to drift causing error in the amount of current flowing into core I. Another important error factor is the relative error between the equipment monitoring and supplying current to both the cores.

Since the transformer displayed drifting tendencies, the arc welder on core II was used as a standard in calculating the relative error between the equipment associated with core I and the equipment associated with core II. These relative error values of per cent accuracy values are listed in the list of equipment. Another possible error factor was introduced in the manner of contact made between the thermistors and the surface of the rod. The thermistors were tied in place by a temperature resistant cloth, thus permitting heat losses. Another source of error was the loss of heat down the thermistor lead wire. To minimize (2) this the leads were positioned as shown in figure 8. The thermistors were placed this way relative to the heat flow to minimize heat losses down the thermistor leads. Another inaccuracy introduced was a result of the sensitivity of the equipment. This largely affected the similitude requirement of proportional control in the two core regions. Of major importance was the extent of human error involved in the collection of the data. All important phases of collecting the data were controlled manually. Where speed was the important requirement, human response was much slower than an equivalent mechanical response. Another important source of error was introduced in the determination of the true peaks of the temperature outputs at points remote to the driver section of the rod. This problem was increased during faster cycle times.

CONCLUSIONS

In conclusion, the model sink frequency was not observed because of two likely possibilities. First it may not be a phenomenon for the thermal model analogy and second the experimental frequency range may have been too narrow to include the possible sink frequency value. The frequency range (5) studied for the occurrence of the sink frequency phenomenon in the UTR-10 was from 10 to 200 cps. The range attainable within the limits of the model study was 0.5×10^{-3} to 6×10^{-3} cps. From figure 1 it can be seen that for the UTR-10, in the same frequency range of 0.5×10^{-3} to 6×10^{-3} cps, the magnitude of the detector response (5) versus frequency is constant. In other words no drop or sink frequency occurs in this frequency range for the UTR-10. This indicates that if the model frequency range were enlarged the phenomenon of the sink frequency could possibly be observed. If such a phenomenon can be observed in the analogous thermal model, true similitude requirements, as calculated earlier, would expand the frequency range to include cycle times in the range of 1.785×10^5 sec or frequencies in the range of 5.6×10^{-6} cps. This range would be very difficult to achieve without making necessary changes in the presented model design.

RECOMMENDATIONS FOR FURTHER STUDY

The thermal analog developed in this research proved to be feasible and similar to the reactor prototype system in many aspects already presented. With more development and refinement of the equipment, it should model frequency response studies well, and give useful information. Some points of interest for further studies are the following,

(a) Further experimental work could involve studies over larger alpha value ranges and greater frequency ranges.

(b) Analytical studies could be made to compare with the experimental results. This would involve using a different set of characteristic equations not based on as many simplifying assumptions and approximations. In this area also, work could be done to develop a transfer function approach for the model, since reactor frequency studies are done in this aspect.

LITERATURE CITED

1. Argonne National Laboratory. Transfer function measurements and reactor stability analysis. Argonne National Laboratory Conf. Proc. 6205. 1960.
2. Beckwith, T. G. and Buck, N. L. Mechanical measurements. 2nd ed. Reading, Massachusetts, Addison-Wesley Publishing Co., Inc. 1969
3. Brown, A. I. and Marco, S. M. Introduction to heat transfer. 3rd ed. New York, N. Y., McGraw-Hill Book Co., Inc. 1958.
4. Glasstone, S. and Sesonske, A. Nuclear reactor engineering. Princeton, New Jersey, D. Van Nostrand Co., Inc. 1967.
5. Hendrickson, R. A. and Murphy, G. Cross-spectral density measurements in a coupled core reactor. Nuclear Science and Engineering 31: 215-221. 1968.
6. Hodgman, C. D., ed. Handbook of chemistry and physics. 39th ed. Cleveland, Ohio, Chemical Rubber Publishing Co. 1958.
7. Ingersoll, L. R. and Zobel, O. J. An introduction to the mathematical theory of heat conduction. Boston, Massachusetts, Ginn and Company. 1913.
8. Lamarsch, J. R. Introduction to nuclear reactor theory. Reading, Massachusetts, Addison-Wesley Publishing Co., Inc. 1966.
9. Merritt, I. W. Spatially dependent frequency response of coupled-core reactors. Unpublished Ph.D. thesis. Ames, Iowa, Library, Iowa State University. 1968.
10. Murphy, G. Similitude in engineering. New York, N. Y., The Ronald Press Company. 1950.
11. Obert, E. F. and Young, R. L. Elements of thermodynamics and heat transfer. 2nd ed. New York, N. Y., McGraw-Hill Book Co., Inc. 1962.

ACKNOWLEDGEMENTS

I would like to acknowledge my major professor, Dr. Glenn Murphy, Head of the Department of Nuclear Engineering, who suggested this research problem and gave me encouragement, assistance, and advice throughout my studies. I would also like to express my appreciation for the Atomic Energy Commission Traineeship which made my study of nuclear engineering possible. Since my research required the use and construction of various pieces of equipment, I would like to express my gratitude to other people who helped me in this aspect, especially people in the Machine Shop, the Instrument Shop, the Electronics Shop, the Engineering Research Institute, the Agricultural Engineering Department, the Ceramic Engineering Department, and the Physics Department. Special thanks goes to Russell Anderson for his aid in this area and also to the students and friends who assisted in the collection of the data.

I wish to acknowledge my parents, the Reverend Mr. and Mrs. John E. Tunstall, for their continued support and encouragement, and especially to my mother for her efforts in typing this thesis.

APPENDIX

List of Symbols and Definitions

A	A constant relating reactor power to the neutron flux
A_0	The peak temperature value in degrees kelvin during a given cycle at an output thermistor location
A_i	The peak temperature value in degrees kelvin during a given cycle at the input driver section thermistor location, position 10
α	A proportionality factor relating temperature to the power generated in the thermal analog core regions
B	The materials buckling, $B^2 = \frac{(1-k) \Sigma_a}{D_1}$
c_1	The specific heat of the thermal analog heat source material
c_2	The specific heat of the thermal analog non-heat source region
D_1	The diffusion coefficient for the reactor fuel region
D_2	The diffusion coefficient for the reactor graphite regions
Σ_a	The macroscopic cross section for absorption
Σ_f	The macroscopic cross section for fission
ϕ	Neutron flux
ϕ_f	Neutron flux in the fuel region of the reactor
ϕ_g	Neutron flux in the graphite region of the reactor
h_1	The film coefficient in the analog heat source region
h_2	The film coefficient in the analog non-heat region
k	Reactor multiplication factor, otherwise the thermal conductivity when in reference to the thermal analog

k_1	The thermal conductivity in the analog heat source region
k_2	The thermal conductivity in the analog non-heat source region
L_T	The diffusion length, $L_T^2 = \frac{D_2}{\Sigma_a}$
n	Neutron density, otherwise in reference to the thermal analog, the proportionality constant between temperature and the neutron flux of the reactor
n_1	The proportionality constant between dimensions in the model and reactor prototype
n_2	The proportionality constant between reactor and model frequencies
P	Power generated in either model or reactor depending on case of reference
Pos	Abbreviation for thermistor position on the model as indicated in figure 8
R	The radius of the analog rod
ρ_1	The density of the thermal analog heat source region material
ρ_2	The density of the thermal analog non-heat source material
ν	The number of neutrons per fission
u	The temperature
u_a	Average temperature of surrounding air
u_f	The temperature in the analog fuel region
u_g	The temperature in the analog non-fuel region
t	Time in prototype
t_m	Time in model

v	The most probable of thermal neutrons, considered constant at 2.2×10^5 cm/sec
w	Abbreviation for watts, a unit of power
ω_m	Frequency in the model system
x	The longitudinal distance reference in prototype
x_m	The longitudinal distance reference in model

Experimental Data and Peak Ratio Calculations

Table 4. Time variation of temperature along the model, trial 1, 20 minute heat pulse cycle

Time (min)	Temperature at these Thermistor Locations (°F)				
	1	2	3	4	5
0	109.0	111.0	116.0	116.5	118.0
1	109.0	110.5	116.0	117.0	118.0
2	109.0	111.0	116.0	117.0	118.5
3	109.5	111.0	116.0	117.0	118.5
4	109.5	111.0	116.0	117.5	119.0
5	110.0	111.5	116.5	117.5	120.0
6	110.0	111.5	117.0	118.5	120.5
7	111.0	112.5	118.0	119.5	122.0
8	112.5	113.5	119.5	121.0	124.5
9	113.0	114.5	120.0	121.5	124.5
10	113.5	115.5	121.0	122.5	125.0
11	114.0	115.5	121.0	122.0	125.0
12	114.0	115.0	120.5	122.0	124.5
13	114.0	115.0	120.5	122.0	124.0
14	113.5	115.5	120.5	122.0	124.0
15	113.5	115.0	120.0	121.5	123.5
16	113.0	115.0	120.0	121.5	122.5
18	113.0	115.0	120.0	121.0	123.0
19	113.0	115.0	120.0	121.0	122.5
20	113.0	114.5	119.5	120.5	122.0
21	112.5	114.5	119.0	121.0	121.0
22	112.5	114.5	119.0	120.0	121.5
23	112.5	114.0	119.0	120.5	121.5
24	112.0	113.5	119.0	120.5	122.0
25	112.5	114.5	119.5	121.0	123.0
26	113.0	115.0	120.0	121.5	124.5
27	113.5	115.5	121.0	123.0	125.0
28	114.0	116.5	122.0	123.5	126.5
29	115.0	117.0	122.5	123.5	126.5
30	115.5	117.5	122.5	124.0	127.0
32	115.0	117.0	122.0	123.0	126.0
33	115.0	117.0	122.0	123.5	126.5
34	115.0	116.5	122.0	123.5	126.0
35	115.0	116.5	121.5	123.0	125.5
36	114.0	116.0	121.0	122.5	125.0
38	114.0	116.0	121.5	122.5	123.5
40	114.0	116.0	121.0	122.0	123.5

Table 4 (Continued)

Time (min)	Temperature at these Thermistor Locations (°F)			
	6	7	8	9
0	122.0	119.0	117.5	74.0
1	121.5	119.0	118.0	74.0
2	122.0	119.0	118.5	75.0
3	122.5	119.5	119.0	77.0
4	123.0	120.0	120.5	80.0
5	124.0	121.0	123.5	87.0
6	126.0	124.0	128.0	95.5
7	128.5	126.5	132.0	103.0
8	130.5	128.5	134.5	105.0
9	131.5	129.5	134.5	104.5
10	131.5	129.0	133.5	103.0
11	131.0	128.5	132.5	100.5
12	130.5	128.0	131.0	98.5
13	129.5	127.0	129.5	96.0
14	129.5	126.5	129.5	94.0
15	128.5	125.5	128.0	91.5
16	128.0	125.5	126.5	90.0
18	128.0	125.0	126.0	88.0
19	127.5	124.5	125.0	87.0
20	127.0	124.5	124.5	86.5
21	126.0	123.5	124.0	85.5
22	126.5	123.5	124.0	85.5
23	126.5	123.5	125.0	87.5
24	127.0	125.0	127.5	94.0
25	129.5	127.0	132.5	103.0
26	131.5	129.5	136.0	108.5
27	133.0	131.0	137.5	111.5
28	134.0	132.0	138.0	112.0
29	134.0	131.5	137.5	110.5
30	133.0	131.0	135.0	106.0
32	132.0	130.0	134.0	103.0
33	132.0	129.0	133.0	101.0
34	131.5	128.5	131.5	99.5
35	131.0	128.0	131.0	96.5
36	130.0	128.0	130.0	95.0
38	129.0	126.5	128.0	91.0
40	128.5	126.0	127.0	89.0

Table 5^a. Time variation of temperature along model I, trial 1, 20 minute heat pulse cycle

Time (min)	Temperature at these Thermistor Locations (°F)				
	1	2	3	4	5
0.0	110.0	113.0	112.0	112.0	110.5
0.5	111.0	114.0	112.0	112.5	111.0
1.0	111.0	114.0	112.5	113.0	
2.0					112.0
2.5	112.5	115.5	113.5	114.0	113.0
3.5	116.0	118.0	116.0	116.0	114.0
4.5	124.0				
5.0	124.1	121.1	121.1	117.5	117.5
6.0	144.0	136.0	132.0	131.0	
6.5					124.0
7.0	163.0	151.0	143.0		
7.5				142.0	133.0
8.5	170.0	157.0	149.0		
9.0				147.0	138.0
10.0	168.0	156.0	149.0	147.0	139.0
11.5	163.0	154.0	147.0	145.0	
12.0	158.0				138.0
12.5		152.0	145.0	143.0	
13.0					136.0
13.5	154.0	149.0	143.0	141.0	
14.0					135.5
14.5	151.0	146.0	141.0	140.0	
15.0	148.0				134.0
15.5		144.0	138.0	138.0	133.0
16.5	145.0	142.0	137.0		
17.0				136.0	131.0
18.0	142.0	139.0	134.0	134.0	130.0
19.0	140.0	138.0	134.0	133.0	129.0
20.0	137.0	136.0	131.5	131.0	127.0
21.0	136.0	135.0	131.0	130.0	127.0
22.5	136.0	134.0	130.0	130.0	
23.0					126.0
23.5	140.0	137.0			
24.0			132.0	132.0	127.0

^aThese tables are only representative of the total experimental data on file in the department.

Table 5 (Continued)

Time (min)	Temperature at these Thermistor Locations (°F)				
	1	2	3	4	5
25.0	158.0	147.0	140.0	139.0	132.0
26.0	177.0	161.0	152.0	149.0	139.0
27.0	191.0	172.0	162.0	157.0	
28.0					146.0
28.5	195.0				
29.0		175.0	165.0	161.0	149.0
30.0	189.5	172.0			
30.5			162.0	158.0	
31.0					148.0
32.0	180.0	168.0	159.0	156.0	147.0
33.0	174.0	164.0	155.0		
33.5				153.0	145.0
34.0	169.0	160.0	153.0	150.0	
34.5					143.0
36.0	156.0	155.0	148.0	146.0	140.0
37.0	156.0	150.0			
38.0			145.0	143.0	137.0
39.0	152.0	147.0	142.0	141.0	136.0
40.0	149.0	145.0	140.0	139.0	134.0

Table 5 (Continued)

Time (min)	Temperature at these Thermistor Locations (°F)				
	6	7	8	9	10
0.0	108.0	105.0	105.0	103.0	98.0
1.0	108.0	105.0	105.0	103.0	99.0
2.0	109.0	106.5	106.0	103.0	101.0
3.0	109.0	106.0	106.0	104.0	107.0
4.0	110.0	108.0	107.5	105.0	121.0
5.0	112.5	110.0	109.5		
5.5				107.0	158.0
6.5	117.0	113.0	113.0		

Table 5 (Continued)

Time (min)	Temperature at these Thermistor Locations (°F)				
	6	7	8	9	10
7.0				110.0	194.0
7.5	123.0				
8.0		120.0	119.0	115.0	
8.5					209.0
9.0	127.0	123.0	122.0		
9.5				118.0	
10.0	129.0				201.0
11.0		125.0	124.0	119.0	191.0
12.0	129.0	125.0	124.5	120.0	182.0
13.0	128.0	125.0	124.0	120.0	175.0
14.0	127.0	123.5	123.0	119.0	168.0
15.0	127.0	123.0	123.0	118.0	162.0
16.0	127.0	123.0	122.5	118.0	157.0
17.0	125.0	121.0	121.0	118.0	
17.5					152.0
18.0	123.0	120.0	119.0	115.0	
18.5					147.0
19.5	122.0	118.5	118.0	114.0	
20.0					143.0
20.5	121.0	117.5	117.5	113.0	
21.0					140.0
21.5	121.0	118.0	117.0	113.5	
22.0					139.0
23.0	120.0	117.0	116.0	112.0	148.0
24.0	120.5				
24.5		117.0	116.0	112.0	
25.0	123.0	119.0			178.0
25.5			118.0	113.5	
26.0					216.0
26.5	128.0	123.0	122.0		
27.0				117.0	244.0
28.0	132.0	127.0	126.5	121.0	248.0
29.0	136.0	131.0	130.0	124.0	
30.0					238.0
31.0	137.8	132.0	131.0		
31.5				125.0	220.0
32.0	136.0	131.0	131.0		
32.5				125.0	
33.0					207.0
33.5	135.0	130.0	130.0	124.5	
34.0					197.0

Table 5 (Continued)

Time (min)	Temperature at these Thermistor Locations (°F)				
	6	7	8	9	10
34.5	134.0	130.0			
35.0			129.0	124.0	188.0
36.5	132.0	128.0	127.0	122.0	
37.0					177.0
38.0	129.5	126.0	125.0		
38.5				120.0	
39.0	129.0	125.0	124.5		165.0
39.5				120.0	
40.0	128.0				160.0
40.5		124.0	124.0	120.0	

Table 6. Time variation of temperature along the model, trial 1, 20 second heat pulse cycle

Time (sec)	Temperature at these Thermistor Locations (°F)			
	1	10	3	10
4	88.0	89.0	92.0	93.0
6	89.0	89.5	93.0	93.0
12	90.0	90.0	93.5	93.0
18	91.0	90.0	94.5	94.0
24	92.0	91.0	95.0	94.0
30	92.5	92.0	96.0	95.0
36	94.0	93.0	96.5	95.5
40	95.5	95.0	97.0	96.5

Table 6 (Continued)

Time (sec)	Temperature at these Thermistor Locations (°F)			
	4	10	5	10
4	95.0	91.0	89.5	92.0
6	96.0	91.5	91.0	92.0
12	96.5	92.0	91.5	93.0
18	97.0	92.0	92.0	93.0
24	98.0	93.0	93.0	94.0
30	95.0	99.0	94.0	93.5
36	95.0	99.5	95.0	94.0
40	95.5	99.5	95.5	94.5

Table 7. Sample of peak I and II ratio calculations
(model II data)

Fre- quency x 10 ⁻³ cps	Peak Ratios for these Thermistor Locations (x 10 ⁻¹)			
	Pos 1		Pos 2	
	Peak I	Peak II	Peak I	Peak II
3.34	9.76	9.60	9.69	9.48
2.78	9.66	9.50	9.57	9.36
2.78	9.70	9.61	9.64	9.49
2.38	9.70	9.53	9.56	9.39
2.08	9.56	9.44	9.43	9.24
2.08	9.59	9.46	9.44	9.26
1.85	9.53	9.44	9.39	9.27
0.83	9.54	9.39	9.36	9.16
0.83	9.54	9.36	9.39	9.15

Table 7 (Continued)

Fre- quency $\times 10^{-3}$ cps	Peak Ratios for these Thermistor Locations ($\times 10^{-1}$)			
	Pos 3		Pos 4	
	Peak I	Peak II	Peak I	Peak II
3.34	9.67	9.41	9.63	9.38
2.78	9.51	9.27	9.48	9.24
2.78	9.61	9.43	9.59	9.39
2.38	9.51	9.31	9.51	9.27
2.08	9.34	9.15	9.30	9.10
2.08	9.38	9.16	9.36	9.12
1.85	9.31	9.15	9.28	9.11
0.83	9.26	9.06	9.24	9.02
0.83	9.30	9.05	9.26	9.00

Table 7 (Continued)

Fre- quency $\times 10^{-3}$ cps	Peak Ratios for these Thermistor Locations ($\times 10^{-1}$)			
	Pos 5		Pos 6	
	Peak I	Peak II	Peak I	Peak II
3.34	9.56	9.30	9.51	9.21
2.78	9.42	9.16	9.34	9.03
2.78	9.53	9.31	9.46	9.22
2.38	9.44	9.19	9.37	9.09
2.08	9.22	8.99	9.13	8.86
2.08	9.27	9.01	9.18	8.90
1.85	9.20	9.00	9.10	8.90
0.83	9.16	8.89	9.04	8.77
0.83	9.18	8.87	9.10	8.75

List of Equipment

1. Scientific Products - Yellow Springs Instrument Company
 - (a) Ten Model No. 427 Thermistors, time constant measured to be 0.7 seconds
 - (b) Model 42SF Tele-Thermometer

Ambient temperature range 32° F to 120° F

Accuracy

0 to 230° F + 1.0° F

-20 to 0° F and 230 to 265° F + 2.0° F

- 40 to -20° F and 265 to 300° F + 3.0° F
 - (c) Model 4002 Switch Box
2. Current Meters
 - (a) General Electric Company - AC Ammeter

Typ p-3 no. 1010558 Capacity 5 amps.

Resistances at 25° C + 0.25% of full scale accuracy
 - (b) General Electric - AC Ammeter

Type p-3 no. 1013466 Capacity 5/10 amps
3. Transformer built by Monty Parker

200 amp ability off of the secondary

Supplied core I of thermal model with current
4. Variac used in conjunction with Monty Parker transformer

Powerstat - Variable Autotransformer Superior Electric Company

Type 2PF 128 input volt - 120 12.5 amps

output volt- 140
5. Transformers for Current Meters - Two, one for each meter

General Electric Model nos. 9jPL

Three turns - ratio 200 to 5

Relative accuracy 30%
6. General Cable Guardian - R-600V, Lead Wire
7. Voltmeters
 - (a) Hewellett-Packard- Model 400C

R.M.S. Volts Range 0.001 - 300 volts
 - (b) Hewellett-Packard-Model 400D

R.M.S. Volts Range 0.001 - 300 volts

Relative accuracy 22%

8. Desk Fans for model cooling
9. Craftsman AC Arc Welder Model No. 245.20101
20 amps - to approx. 190 amps
Supplied core II with current
10. Power Supply - Electro Products Lab Model D-612T
Filtered DC power supply
voltage scale: 0 - 20 volts dc
amp scale: 0 - 10 amps
output: 0 - 16 volts 10 amps continuous duty
This was used to drive the heat pulse section of the
model